PNAS
www.pnas.org

Supplementary Information for

Motor Neuron Disease-Associated Loss of Nuclear TDP-43 is Linked to DNA Double-Strand Break Repair Defects

Joy Mitra[a], Erika N. Guerrero[a,b,c], Pavana M. Hegde[a], Nicole F. Liachko[d,e], Haibo Wang[a,n], Velmarini Vasquez[a,b,c], Junling Gao[f], Arvind Pandey[a], J. Paul Taylor[g,h], Brian C. Kraemer[d,e], Ping Wu[f], Istvan Boldogh[i], Ralph M. Garruto[j,k,l], Sankar Mitra[a,l], K.S. Rao[b] and Muralidhar L. Hegde[a,l,m,n,l]

[a]Department of Radiation Oncology, Houston Methodist Research Institute, Houston, TX 77030; [b]Center for Neuroscience, Instituto de Investigaciones Científicas y Servicios de Alta Tecnología (INDICASAT AIP), City of Knowledge, Republic of Panama; [c]Department of Biotechnology, Acharya Nagarjuna University, Guntur, India; [d]Geriatric Research Education and Clinical Center, Veterans Affairs Puget Sound Health Care System, Seattle, WA, 98108; [e]Division of Gerontology and Geriatric Medicine, Department of Medicine, University of Washington, Seattle, WA, 98104; [f]Department of Neuroscience and Cell Biology, University of Texas Medical Branch, Galveston, TX 77555; [g]Department of Cell and Molecular Biology, St. Jude Children's Research Hospital, Memphis, TN 38105; [h]Howard Hughes Medical Institute, Chevy Chase, MD 20815; [i]Department of Microbiology and Immunology, University of Texas Medical Branch, Galveston, TX 77555; [j]Departments of Anthropology and Biological Sciences, Binghamton University, Binghamton, NY 13902; [k]State University of New York, Binghamton, NY 13902; [l]Weill Medical College, New York, NY 10065; [m]Houston Methodist Neurological Institute, Houston, TX 77030; [n]Institute of Academic Medicine, Houston Methodist, Houston, TX 77030

[1]Corresponding Authors: Muralidhar L. Hegde mlhegde@houstonmethodist.org
Ralph M. Garruto rgarruto@binghamton.edu

***SI Appendix* includes:**

Supplementary text (*SI* Results, *SI* Discussion, *SI* Materials and Methods)
Tables S1 to S3
References cited in *SI* Text
Figs. S1 to S13

SI Results

Validation and Specificity of anti-TDP-43 antibody

The co-IP and PLA analyses were performed in neuronal cells after TDP-43 knockdown (KD) to validate the specificity of the anti-TDP-43 Ab. The immunoblots (IB) of TDP-43 co-IP from control and TDP-43 siRNA transfected cells were probed for γH2AX, p-ATM, p-53BP1 and XRCC4, whose levels were reduced after TDP-43 KD (*SI Appendix,* Fig. S3*E*). siRNA was transfected for 72 h to obtain ~80% KD of TDP-43 (*SI Appendix,* Fig. S6*A*). The Ab specificity in PLA was confirmed by the loss of PLA signals for TDP-43 vs. Ku70 or 53BP1, from etoposide-treated and TDP-43 KD NP cells (*SI Appendix,* Fig. S3*F*). These control experiments confirmed that the protein co-eluted with anti-TDP-43 Ab was indeed TDP-43.

TDP-43 is required for optimal DSB repair via NHEJ in neurons

Following up our results demonstrating reduced DSB repair via NHEJ using an I-Sce I approach (Fig. 4*C-E*), we confirmed this using a second custom-generated, physiologically relevant blocked-termini-DSB-containing plasmid assay (1). It is important to note that I-SceI-induced DSB repair may provide a gross underestimate of repair events as it contains clean DSB termini, unlike a majority of endogenous DSBs generated in cells, which invariably contain unligatable blocked termini. To overcome this, in the second approach, we generated the pNB1GFP reporter plasmid with a single DSB flanked with 3'P unligatable termini, formed by cleaving a U•U pair-harboring GFP-plasmid with *E. coli* DNA glycosylase Fpg (schematically shown in *SI Appendix,* Fig. S8*G*) (1). The repair of linearized pNB1 was first evaluated *in vitro* by incubating with the nuclear extracts from control or TDP-43 siRNA-transfected neuronal cells and analyzed in 1% agarose gel electrophoresis (*SI Appendix,* Fig. S8*H*). Partial re-circularization (~60%) of pNB1 was observed with the control nuclear extract, however, TDP-43-depleted nuclear extract generated only <10% re-circularization (*SI Appendix,* Fig. S8*I*). The re-circularized pNB1 products were characterized by amplification in XL-10 gold *E. coli* to screen for their colony-forming efficiency against ampicillin selection, which further confirmed marked reduction in number of colonies in TDP-43-depleted samples (*SI Appendix,* Fig. S8*H*, *Bottom* panel). The repair of the linearized pNB1 plasmid was also evaluated for *in cellulo* re-circularization by transfecting into SH-SY5Y cells pre-treated with control or TDP-43 siRNA, followed by IF, which showed ~60% reduction in the number of GFP+ve cells compared to that of the control siRNA treated cells (*SI Appendix,* Fig. S8*E*). The repaired plasmid was then isolated from the SH-SY5Y cells, 6 h after transfection as Hirt supernatant (2), which was then used to transform in the XL-10 *E. coli.* Individual plasmid DNA from 20 independent colonies were sequenced to characterize the sequence at repaired joint. Sequence analysis confirmed the DSB repair in ~85% of plasmids occurred via error-free NHEJ, while ~15% showed a single base deletion at the DSB site (*SI Appendix,* Fig. S8*J*). In summary, these results show that loss of TDP-43 inhibits NHEJ in the neuronal genome.

SI Discussion

Metabolically active neurons with high transcriptional activity are continuously exposed to various types of genome damage, whose efficient repair is critical for maintaining the genomic integrity of these long-lived and poorly replenishable cells in adult humans (3, 4). Contrary to the prevailing notion that the most common types of damage in the neuronal genome are reactive oxygen species (ROS)-induced oxidized bases and SSBs, recent studies show that DSBs may be induced by as yet uncharacterized endogenous sources and repaired efficiently under normal physiological condition

(5-7). For example, Lenart Mucke and colleagues showed that increasing metabolic activity in mice by exercise leads to transient formation of DSBs, a process exacerbated in presence of Aβ peptides (8). Other studies suggested that localized formation of ROS by demethylases in the proximity of gene promoter sequences during gene activation produces robust oxidative damage to DNA, which may be required for resolving topological constraints for neuronal gene expression (5). Wallace and colleagues have independently shown that bi-stranded accumulation of unrepaired induced oxidative damage can cause secondary DSBs (9, 10). Furthermore, several studies recently demonstrated that defects in DSB repair pathways in subsets of FUS or C9*orf*72-linked ALS cause accumulation of unrepaired DSBs, likely generated by endogenous sources (11-13). Cumulatively, these studies suggest that DSBs can be generated endogenously in post-mitotic neurons, whose efficient repair is critical for maintaining genome fidelity.

Although, TDP-43 does not bind to biotinylated DNA ends *in vitro*, our *in cell* data show that TDP-43 associates with DSB sites generated by IR or etoposide, as part of a complex with other DSB response and repair proteins. While etoposide generates TOPO-II-linked 5′-DSB adducts, these covalently blocked termini are enzymatically processed by DNA-2/TDP-2 in mammalian cells to generate 5′P clean ends for downstream repair process (14, 15). Alternatively, the TOPO-II-linked termini may also be removed by nuclease activity of MRN complex together with CtIP (16, 17). This reaction is believed to occur very early in the DDR process of etoposide induced DSBs, before the downstream DSB repair factors are assembled. It is likely that, although TDP-43 is present as part of DDR complex, it binds the termini after the TOPO-II-blocked ends are removed.

Consistent with our model, growing evidence from various studies has linked a deficiency in DSB repair response components to neurodegenerative phenotypes, including Alzheimer's disease (18), Parkinson's disease (19), ALS (20), and premature aging diseases, such as progeroid syndromes (21). Mutations in key DSBR proteins (e.g., ATM in ataxia telangiectasia; NBS1 in Neijmegen breakage syndrome; PNKP in MCSZ; and MRE11 in A-TLD) have been shown to predispose humans to the neurodegenerative phenotype, underscoring the importance of DSBR for post-mitotic neurons (4).

The role of RDBPs in DNA repair has been recently highlighted in a rapidly increasing number of studies. Another RNA/DNA-binding protein, fused in sarcoma/translocated in liposarcoma (FUS/TLS), linked to the ALS-FUS subtype has been shown to participate in DSB repair, and pathogenic mutations in this protein induce genome damage in neurons (13, 20). It is important to note that FUS and TDP-43 pathologies are rarely seen in an ALS patient (except in one case study showing mutations in both FUS and TDP-43 genes, but with moderate FUS pathology and no TDP-43 pathology (22). More recently, we have documented hnRNP-U, a member of the hnRNP family, acts as a switch allowing DSB repair to proceed in preference to oxidative/SSB repair processes (23, 24). Notably, TDP-43, FUS, and hnRNP-U have been found to interact with each other. Other studies have linked the involvement of hnRNP-A1 and hnRNP-U-like protein variants in DDR (25, 26). Furthermore, in view of a recent study, which identified a DSB repair defect in C9*orf*72-linked ALS patients, it will be interesting to elucidate any potential cross-talk of TDP-43 and C9*orf*72 pathologies. DSB repair defects in C9*orf*72-ALS was suggested to occur due to altered R-loop processing at G quadruplex structures and expanded hexanucleotide repeat sequences (12, 27, 28). Studies have also shown the involvement of both short and long non-coding RNA in DSB repair, and multiple models have been proposed to describe the involvement of small RNAs in DDR, including the possibility of their acting as the template for error-free repair (29, 30). It is also likely that the RNAs together with RDBPs may act as scaffold

or glue for the large, dynamic repair complex at the damage sites. Further investigation along these lines can add new paradigm to our knowledge of DSB repair systems and their defects in TDP-43-associated neurodegenerative diseases and provide avenues for DNA repair-based therapies.

SI Materials and Methods

Cell culture.
Human neuroblastoma SH-SY5Y cells (ATCC) or HEK293 (ATCC) cells were cultured in DMEM/F12 media (Gibco) or DMEM High glucose (Gibco) with 10% Fetal Bovine Serum (Sigma) and 1% Penicillin-Streptomycin (Sigma) at 37 ˚C with 5% CO_2. SH-SY5Y cells were differentiated in with Retinoic acid (RA) (10 μM) and BDNF (50 ng/mL) in DMEM/F12 and 1% FBS for 4 to 6 days (31, 32).
Human Neural Stem Cell (hNSC) culture and differentiation into spinal motor neurons. A normal iPSC line KYOU-DXR0109B (201B7) was obtained from ATCC and grown in CellMatrix basement membrane gel (Gibco) and Pluripotent Stem Cell SFM XF/FF media (Gibco) at 37 °C and 5% CO_2.Human fetal (8-10 weeks) cortical neural stem cell (33) line K048 was cultured as described before (34). Briefly, the cells were expanded as neurospheres at 3-6 x 10^6 cells/T75 flask containing growth medium (DMEM-F12 3:1; HEPES 1.5%; 10% glucose 1.5% and Pen-Strep 1%) along with EGF, bFGF, LIF, insulin, heparin, N2 and glutamine and passaged every 9-10 days. For priming, small spheres (2-3 days post-passage) of 6 x 10^4 cells/cm^2 were plated onto 0.01% Poly-D-Lysine and 1μg/cm^2 mouse laminin (Life technologies), and incubated with FHL priming media containing N2, insulin (1:400), 20 ng/ml bFGF, 5 μg/ml heparin, 1μg/ml laminin and 2 mM Glutamax-I. Cells were primed in bFGF/heparin/laminin for 4 days. For differentiation of primed cells to motor neurons, cells were incubated with basic medium plus B27 supplement (1:50) for 9-12 days, changing ½ media every 3-4 days.
Human iPSC to Neural Progenitor cells. Derivation of NPCs was done using PSC neural induction medium (Gibco) as described previously (35). Briefly, E8M was replaced with neural induction medium approximately 24 h after passaging iPSCs, which were maintained in this medium for 7 days. On day 7 of neural induction, NPCs (P0) were passaged into Geltrex (Gibco)-coated 6-well plates and expanded in StemPRO neural stem cell SFM media. Neural induction efficiency was tested at passage 3 by immunofluorescence staining with a pluripotent marker (Oct4) and neural lineage stem cell marker (Nestin) as described before (36)
Human iPSC to differentiated motor neurons. Briefly, iPSC clones were suspended and transferred from a 60-cm dish into a T-25 flask with neuronal basic medium (mixture of 50% Neurobasal medium and 50% DMEM/F12 medium, with N2 and B27 supplements without vitamin A), following collagenase type IV digestion. After 2 days incubating with 5 μM ROCK Inhibitor (Y-27632, RI, from Merck Millipore), 40 μM TGF- β inhibitor (SB 431524, SB, Tocris Bioscience), 0.2 μM bone morphogenetic protein inhibitor (LDN-193189, LDN, from Stemgent), and 3 μM GSK-3 inhibitor (CHIR99021, CHIR, from Tocris Bioscience), suspended cell spheres were then incubated with a neuronal basic medium containing 0.1 μM retinoic acid (RA, from Sigma) and 500 nM Smoothened Agonist (SAG, from Merck Millipore) for 4 days. Cells were then incubated for 2 days in a neuronal basic medium containing RA, SAG, 10 ng/ml Brain-derived neurotrophic factor (BDNF, from Peprotech), and 10 ng/ml Glial cell-derived neurotrophic factor (GDNF, from Peprotech). Cell spheres were then dissociated with a neuronal basic medium containing trypsin (0.025%)/DNase in water bath for 20 min at 37 °C, and then were pipetted into single cells with the medium containing trypsin inhibitor (1.2 mg/ml). After cell counting, a defined number of cells were seeded into 20 μg/ml Laminin (Life technologies) -coated dishes or chamber slides and incubated for 5 days in a neuronal basic medium containing RA, SAG, BDNF, GDNF, and 10 μM DAPT, then incubated for 2 days in a neuronal basic medium containing BDNF, GDNF, and 20 μM Inhibitor of γ-secretase (DAPT, from Tocris Bioscience). For motor neuron maturation, cells were then kept for over 7 days in a medium containing BDNF, GDNF, 10 ng/ml ciliary neurotrophic factor (CNTF, from Peprotech).

Expression Plasmids

FLAG-TDP-43 pcDNA 3.1(+) mammalian expression plasmid was described previously (37). TDP-43 bacterial expression plasmid was constructed by directional cloning of PCR amplified TDP-43 coding DNA sequence with forward primer TDPF-NdeI : 5'-GGGCATATGTCTGAATATATTCGGGTAACC-3' and reverse primer TDPR-EcoRI : 5'-CCGGAATTCCTAGTGATTCATTCCCCAGCC-3' at NdeI / EcoRI restriction sites in pET28a bacterial expression plasmid in-frame with His-tag. pcDNA3.1-TDP-43 plasmid was used as the template for this PCR amplification.
pcDNA3.1(+)-FLAG-TDP43-NLS-1 and pcDNA3.1(+)-FLAG-TDP43-NES-1 mutant plasmids were generated by site-directed mutagenesis using QuickChange II Site-directed Mutagenesis kit per manufacturer's protocol. Following primers were used for these reactions:
NLS1-F: 5'-CAACTATCCAAAAGATAACGCAGCAGCAATGGATGAGACAGATGC-3'
NLS1-R: 5'-GCACCTGTCTCATCCATTGCTGCTGCGTTATCTTTTGGATAGTTG-3'
NES1-F: 5'-GCAGATGATCAGGCTGCGCAGTCTGCTTGTGGAGAGGAC-3'
NES1-R: 5'-GTCCTCTCCACAAGCAGACTGCGCAGCCTGATCATCTGC-3'

Generation of inducible CRISPR-mediated TDP-43 knockout (KO) line
Single-guide RNA (sgRNA) against TDP-43 gene was designed by screening target sequence with online tool http://www.broadinstitute.org/rnai/public/analysis-tools/sgrna-design. Two high-score sgRNA target sequences (sgRNA1 – Sense strand: 5'-GGTTACAGCCCAGTTTCCAG-3' and sgRNA2 – Antisense strand: 5'-GCAGAATTCCTTCCACCAGT-3') were selected towards the 5'-end of TDP-43 CDS. Each sgRNA module was generated by overlapping PCR protocol as described previously with minor modifications (38), and both of the sgRNA modules were cloned into the same pLX-sgRNA vector by a modified cloning strategy, where sgRNA1 module was digested with XhoI/BamHI and sgRNA2 with BamHI/NheI restriction enzymes. Then, both modules were cloned simultaneously in XhoI/NheI digested lentiviral pLX-sgRNA plasmid. Transfection of Humanized Cas9 containing lentiviral pCW-Cas9 and customized pLX-sgRNA plasmids in to SH-SY5Y cells, followed by cell selection and induction of TDP-43 knockout were performed as described previously (39).
Primers use to amplify U6 promotor target sgRNA sequence and terminator sequence:
Outer primer F1: AAACTCGAGTGTACAAAAAAGCAGGCTTTAAAG
Outer primer R2: AAAGCTAGCTAATGCCAACTTTGTACAAGAAAGCTG
sgRNA1_R1: CTGGAAACTGGGCTGTAACTCGGTGTTTCGTCCTTTCC
sgRNA1_F2: GAGTTACAGCCCAGTTTCCAGGTTTTAGAGCTAGAAATAGCAA
sgRNA2_R1: ACTGGTGGAAGGAATTCTGCGGTGTTTCGTCCTTTCC
sgRNA2_F2: GCAGAATTCCTTCCACCAGTGTTTTAGAGCTAGAAATAGCAA
Sequencing primers for pLX-sgRNA:
Forward: CGGGTTTATTACAGGGACAGCAG
Reverse: TACCAGTCAATCTTTCACAAATTTTGT

TDP-43 knockdown (KD)
siRNA: SH-SY5Y or neural progenitor cells were transfected with 100nM TDP-43 (NM_007375.3) siRNA oligos (Sigma, Forward: 5'-GAGACUUGGUGGUGCAUAA-3'; Reverse: 5'-UUAUGCACCACCAAGUCUC-3') or scrambled control siRNA oligos (Santa Cruz Biotechnology). A ~ 80% KD of TDP-43 was observed 48 post transfection. For KD of endogenous TDP-43, while allowing its ectopic expression, a 3´-UTR-region of *TARDBP* gene (Sigma: sequence) was used. Transfection of undifferentiated SH-SY5Y cells was performed using lipofectamine-2000, per standard protocol. For transfection of differentiated neurons was carried out using a 4th generation electroporation (Amaxa) in a 24-well plate (on coverslip as required) following the manufacturer's protocol. Electroporation in 4th generation Amaxa, allows transfection of adherent cells without the need to suspend the cells in cuvette, thus minimizing cell death due to mechanical injury.
shRNA, lentiviral packaging and transduction: Lentiviral shRNA vectors against *TARBBP* gene were purchased from GeneCopoeia. The KD efficiency of the four individual shRNA provided was tested by lipofectamine-mediated transient transfection of each shRNA in SH-SY5Y cells. shRNA-2 showed >80%

KD efficiency, which was used in further experiments. The lentiviral shRNA particles were generated using Lenti-vpak kit following manufacturer's protocol. Briefly, ~2.5 x 10^6 HEK293T cells were plated onto poly-D-lysine coated 10cm petri-dish 1 day prior to transfection. Desired lentiviral vectors were transfected along with packaging plasmids per the protocol of 3rd generation packaging kit. Viral supernatants were collected at 18, 24 and 48 h post-transfection time-point and stored at 4 °C during collection. Collected supernatants were passed through 0.45 µm syringe filter to remove cellular debris, and concentrated by mixing 1 volume of Lenti X-concentrator with 3 volumes of clarified supernatant and kept at 4 °C overnight. The mixture was centrifuged at 10,000 rpm for 30 min at 4 °C. The pellet was suspended in 1/100th of original volume in PBS, then titrated using Lenti-X GoStix per the protocol and stored at -80 °C in multiple aliquots.
Neural progenitor cells or differentiated motor neurons were transduced with adequate amount of shRNA-2 or control shRNA lentiviral particles in combination with 8 µg/ml polybrene in respective growth medium for 24 h. After that, cells were washed with DPBS and cultured with regular growth medium.

Total cellular and nuclear protein extraction
Cells harvested with cell scrapers, were pelleted at 1,500 rpm at 4˚C for 5 minutes and lysed with whole cell lysis buffer (50 mM Tris-HCl pH 7.5, 150 mM NaCl, 1 mM EDTA and protease inhibitor), or subcellular fractionation using sequential lysis buffers -Cytoplasmic extraction buffer (10 mM Tris-HCl pH 7.5, 0.34 M Sucrose, 3 mM $CaCl_2$, 2 mM $MgCl_2$,0.1 mM EDTA, 1 mM DTT, 0.1% Nonidet P-40 and protease inhibitor), Nuclear extraction buffer (20 mM HEPES, 3 mM EDTA, 10% Glycerol, 150 mM potassium acetate, 1.5 mM $MgCl_2$, 1 mM DTT, 0.5% Nonidet P-40 and protease inhibitor), Chromatin extraction buffer (150 mM HEPES, 1.5 mM $MgCl_2$, 150 mM Potassium acetate, 10% Glycerol and protease inhibitor) as described previously (40).

Immunoblotting (IB)
Proteins eluted from co-IP were separated on a NuPAGE 4-12% Bis-Tris Gel. Proteins were electro-transferred in a nitrocellulose 0.45 µm pore size membrane in 1X NuPAGE transfer buffer. After blocking in 5% skimmed milk solution with 1% Tris-Buffered saline with Tween 20 (TBST) buffer, the membranes were immunoblotted with appropriate antibodies (For details see *SI Appendix*, Table S3) was done in 1% skimmed milk and washed 3 times with 1% TBST.

Co-immunoprecipitation (co-IP)
Endogenous TDP-43 co-IP was performed using Protein A/G PLUS agarose beads (Santa Cruz Biotechnology). Cells were harvested and lysed with 0.2% NP-40, 150 mM NaCl, 25 mM Tris-HCl and 0.1% SDS. Lysate was precleared by adding by adding 1 µg of protein of IgG along with protein A/G beads incubate at 4 °C for 30 min and collect the supernatant and incubate with the suitable primary antibody. After incubation, the protein A/G beads were added, incubated for 1 hour in a rocker platform and centrifuge at 2,500 rpm. Posterior to three washes the protein complex was eluted from the beads.
For co-IP with ectopically expressing FLAG-TDP-43, neuronal cells were transfected with expression plasmids using lipofectamine 2000 (Invitrogen) and Opti-MEM I (1X) (Gibco). 48 h post transfection, cells were scrape-harvested and lysed in TBS buffer (50 mM Tris-HCl p.H 7.5, 150 mM NaCl, 1 mM EDTA and protease inhibitor cocktail) and centrifuged at 10,000 rpm for 10 min. The extract was treated with Benzonase for 30 min at 37 ºC and incubated on a shaking rocker for 3 h at 4 °C and immunoprecipitated with FLAG-M2 agarose beads collected by centrifugation. Posterior to three washes with cold Tris-buffered saline (TBS) TDP-43-FLAG protein was eluted from the beads.

Recombinant TDP-43 expression and purification
The human recombinant TDP-43 was purified from the extract of His-tag-TDP-43-pET28a plasmid-bearing *E. coli* by sequential Ni-column and cation exchange chromatography. Briefly, the His-tag-TDP-43-pET28a plasmid was transformed in BL21-RIPL *E. coli* strain by heat shock at 42 ^{0}C for 45 s and cultured in suspension flask until the absorption at 600nm reaches 0.6, followed by induction by IPTG (2 mM) at

16 ^{0}C for 20 h. His-tag TDP-43 was purified from the bacterial lysate as described elsewhere (24). The purity of protein was confirmed by SDS-PAGE analysis.

Biotin affinity co-elution

For affinity co-elution assay, a duplex and nicked duplex oligos, distinctly biotinylated at one or both ends of complementary oligo were purchased from Sigma. The oligos were annealed by gradual cooling in a boiling water bath to generate a duplex oligo. Biotinylated oligo at a final concentration of 10 μM was mixed with 1 μg recombinant TDP-43 in PBS and incubated at 30 ºC for 15 min with gentle shaking. The affinity pull-down was performed with Streptavidin-coupled Dynabeads^{TM} M-280 (Thermo Scientific) following the manufacturer's protocol. The eluted protein product was tested by immunoblotting using anti-TDP-43 antibody.

Damaged DNA Immunoprecipitation (dDIP)

Neuronal cells differentiated using a mixture of Retinoic Acid and Brain-derived neurotrophic factor (RA/BDNF). To promote DNA strand breaks cells were treated with IR (3 Gy). Damaged DNA Immunoprecipitation protocol was followed as previously described (41). DSB sites in genome were labeled by terminal deoxynucleotidyl transferase-mediated dUTP-biotin end-labeling (TUNEL) using Biotin-16-dUTP (42) as per manufacturer's protocol. To suppress the TdT reaction 200 mM EDTA was added. Cells were harvested with PBS, lysed and sonicated before performing Chromatin Immunoprecipitation (ChIP) as described below. The sonicated and cleared lysate using 5 μg of anti-Biotin antibody or anti-TDP-43 antibody and Magna ChIP Protein A Magnetic beads (Millipore). Labeled DNA was purified using standard Phenol/Chloroform protocol. Purified DNA was dissolved in 10 mM Tris-HCl pH 8 and quantification was done using SYBR GREEN-based Real Time PCR (Applied Biosystems, 7500).

Chromatin Immunoprecipitation (ChIP)

ChIP assay was performed following previously published protocol (39). Briefly, control or TDP-43 siRNA transfected cells were treated with DMSO or etoposide (10 μM) for 4 h. Then, cells were crosslinked in 1% formaldehyde at room temperature for 20 min. The crosslinking reaction was quenched with 125 mM glycine, and cells were harvested with cold 1X PBS/ 1X protease inhibitor buffer. Chromatin was sonicated to an average fragment sizes of 250-650 bp.

For γH2AX ChIP/re-ChIP assay, γH2AX ChIP was performed with cleared lysates by incubating with 5 μg of mouse IgG or γH2AX antibody (1:1000) and the Magna ChIP Protein A magnetic beads overnight at 4 ºC. For re-ChIP assay, γH2AX ChIP products were eluted in 1% SDS and 100 mM $NaHCO_3$ at room temperature for 15 min with 1X protease inhibitor cocktail. Re-ChIP was performed with rabbit anti-53BP1 (1:1000) and mouse anti-XRCC4 (1:200) antibody along with respective IgG controls and the Magna ChIP Protein A magnetic beads overnight at 4 ºC. All the ChIP eluates were subjected to reverse-crosslinking, purification by phenol/chloroform extraction and finally dissolved in 10 mM Tris-HCl (pH 8). Relative occupancy of the target protein at chromosome-wide damage sites was analyzed by qPCR with primers (sequences given below) targeting *HPRT* gene.

HPRT_250F: 5′- TGCTCGAGATGTGATGAAGG -3′
HPRT_250R: 5′- CTGCATTGTTTTGCCAGTGT -3′

To analyze DSB occupancy of proteins at I-SceI cut site, ~ 1 x 10^6 cells were first transfected with pimEJ5GFP NHEJ reporter plasmid with and without KD of TDP-43, followed by a second transfection with I-SceI expression plasmid. NHEJ reporter harboring cells with or without I-SceI expression were processed, as described before, at 5 h post-I-SceI transfection. Input samples were first normalized with primers amplifying 260 bp on GFP coding sequence. ChIP assay was set up with mouse IgG or anti TDP-43/XRCC4 antibody and Magna ChIP Protein A beads at 4 ºC for 6 h. The relative occupancy at DSB for TDP-43 or XRCC4 was measured by qPCR analysis with GFP specific primers flanking the I-SceI recognition site.

GFP-260_F: 5′- ATGGTGAGCAAGGGCGAGGAGCTGTTCAC -3′
GFP-260_R: 5′- GACTTGAAGAAGTCGTGCTGCTTCATGTGG -3′

***In vitro* His- affinity pulldown assay**
His affinity pulldown co-elution (pulldown) assay was carried out as previous described (43, 44). Briefly, purified XRCC4 and Lig4 protein complex (100 pmole) was mixed with His-tagged TDP-43 (40 pmole), which was pre-bound to HisPur magnetic nickel-nitrilotriacetic acid (Ni-NTA) beads and incubated for 1 h at 4ºC with continuous rotation in a buffer containing 1X TBS, 5% BSA and 10% glycerol. Beads were washed with TBS containing 0.1% Triton X-100 and 300 mM NaCl, and the bound proteins were eluted with SDS sample dye and subjected to western blot analysis for presence of XRCC4 and Lig4 proteins using respective antibodies.

Immunofluorescence (IF) microscopy
hNSC-derived motor neurons, neural progenitor and SH-SY5Y cells were cultured in 8 well chamber slides (Millicell EZ slides, Millipore) were fixed in 4% paraformaldehyde in phosphate-buffered saline (PBS) for 20 minutes and permeabilized with 0.2% Tween 20 in PBS for 20 minutes at room temperature. Blocking was performed with 3% BSA solution in DPBS for 30 minutes. Incubation was done with appropriate primary antibodies (For details see *SI Appendix*, Table S3) overnight at 4 ˚C in 1% BSA solution and fluorescent secondary antibodies for 1 h at 37 ˚C in 1% BSA solution. Slides were washed 3 times and counterstained with DAPI. Images were captured in AXIO Observer inverted microscope (Carl Zeiss).

Proximity ligation Assay (PLA)
iPSC-derived motor neurons or neural progenitor cells cultured on 8 well chamber slides (Millicell EZ slides, Millipore) were fixed in 4% paraformaldehyde in phosphate-buffered saline (PBS) for 20 min and permeabilized with 0.2% Tween 20 in PBS for 20 min at room temperature. In situ protein-protein association was analyzed using PLA (Duolink) as per manufacturer's instructions; PLA is an antibody-based method that detects molecules in close proximity (~16 nm). Images were analyzed in AXIO Observer inverted microscope (Carl Zeiss) (45, 46).

Single Cell Gel Electrophoresis (Comet) Assay
Alkaline and Neutral Comet assay was performed in motor neurons at 96 h after TDP-43 depletion according to manufacturer's protocol (TREVIGEN). Briefly, NP cells were mixed with low-melt agarose (TREVIGEN) and placed in Comet assay slides (TREVIGEN). Slides were immersed in neutral and alkaline electrophoresis buffer respectively after immersion in lysis solution (TREVIGEN). For Alkaline Comet Assay slides were subjected to electrophoresis at 21 V for 30 min; while for Neutral Comet Assay the slides were subjected to electrophoresis at 21 V for 45 min at 4 °C. Slides were fixed with 70% ethanol and stained with SYBR® Green and visualized in EVOS FL auto fluorescence microscope (life technologies).

ApopTag®Peroxidase *In situ* Apoptosis Detection Kit TUNEL staining
In situ DNA strand breaks staining in cultured cells or postmortem brain/spinal cord cervical tissue sections of ALS patients and control brain tissue by labeling of free 3'OH DNA by terminal deoxylnucleotidyl-transferase-mediated dUTP-nick end labeling was done following manufacturer's protocol (Millipore).

Live cell imaging of micro-irradiation based DSB repair
For live cell imaging of DSB repair in NP cells, cells were seeded on gridded glass coverslips (MatTek) followed by transfection with TDP-43-tdTOMATO or Ku70-GFP reporter plasmids. Cells were pre-sensitized with 100 nM Hoechst 33342 for 10 min. A Zeiss LSM780 laser-scanning confocal microscope equipped with a 63X, 1.4 NA Plan-Apo oil-immersion objective was used for all micro-irradiation experiments. DSBs were generated in a laser ablation track in the region of interest (ROI) by 405 nm diode laser set to 100% transmission output for 150 iterations. Following irradiation, cells were maintained for

designated time periods scanning the fluorescence intensity of the laser-track for 30 min with 1 min interval. For each assay, data were collected from 5–15 cells and the signal intensities in the irradiated area were measured by ImageJ and normalized to the signal of the whole nucleus (20, 47).

Quantitation of DNA strand breaks by Long Amplicon PCR (LA-PCR) based assay

Genomic DNA was isolated from NPC or SH-SY5Y cells with or without TDP-43 downregulation using DNeasy Blood and tissue kit (Qiagen) per manufacturer´s directions. DNA was quantified using SYBR GREEN-based Real Time PCR (Applied Biosystems, 7500). To evaluate accumulation of strand breaks using LongAmp *Taq* DNA polymerase (New England Biolabs) a ~10.9 kb genomic DNA region (*HPRT* gene, exons 2-5, Accession number J00205) was amplified using the suitable primers (forward: 5'-TGGGAT TACACGTGTGAACCAACC-3'; reverse; 5'-GCTCTACCCTGTCCTCTACCGTCC-3') (48). Preliminary assays were carried out to ensure linearity of PCR amplification in respect to the number of cycles and DNA concentration. As a control, a shorter fragment of ~250 bp was also amplified using suitable primers (forward: 5'-TGCTCGAGATGTGATGAAGG-3'; reverse: 5'-CTGCATTGTTTTGCCAGTGT-3') (49).

For LA-PCR from ALS patient's spinal cord tissues, snap-frozen spinal cord tissues were ground in liquid nitrogen to fine powder form. 20 mg of tissue powder were used for each sample to extract high quality genomic DNA using genomic-tip 20/G kit per the manufacturer's direction. The thermal cycling profile and DNA concentrations were optimized prior to setting up the actual reaction. 20 ng of genomic DNA were used for each sample for LA-PCR assay using the optimized thermal profile 94 °C for 30 s (94 °C for 30 s, 59 °C for 30 s, 65 °C for 10 min) for 25 cycles and 65°C for 10 min (50). The primers for *pol* β gene

Forward: 5´- TATCTCTCTTCCTCTTCACTTCTCCCCTGG-3´

Reverse: 5´- CGTGATGCCGCCGTTGAGGGTCTCCTG-3´

were used to amplify ~12.3 kb genomic region for LA-PCR assay. Internal primer pair (forward: 5´-TATGGACCCCCATGAGGAACA-3´; reverse: 5´- AACCGTCGGCTAAAGACGTG -3´) was used for normalization of template DNA across the samples. PCR products were separated in agarose gel and visualized using Gel Logic 2200 imagining system (Kodak) and amplified product was quantitated by dsDNA Picogreen assay as described elsewhere (45).

Cell death/Survival Assays

MTT assay: Treated or untreated NPC or SH-SY5Y cells exposed to IR (3 Gy) were seeded in a 96-well ELISA plate (Corning) in triplicates and incubated 48 h post treatment. MTT assay was performed following manufacturer's protocol (TREVIGEN). In summary, 10 µl of MTT reagent was add to each well and incubated for 2 to 4 h until purple dye is visible then 100 µl of detergent reagent (TREVIGEN) was added. After 2 to 4 h of incubation absorbance at 570 nm was measure in a microplate reader (Bio-Rad, 680 XR).

Annexin V/PIFlow cytometry: The level of apoptosis in inducible TDP-43 KO CRISPR cells was measured at 0, 2, 4 and 6 days after Dox induction using the FITC-Annexin V apoptosis detection kit. Flow-cytometric analysis of apoptotic cell death was performed as indicated earlier (51). Briefly, cells were harvested, washed with PBS, and incubated with fluorescein isothiocynate (FITC) conjugated Annexin V and propidium iodide (PI) according to the instruction of Annexin V apoptosis detection kit. A total of 10,000 events were acquired per sample by fluorescence activated cell sorting (FACS) and analyzed using Flowjo software (Becton-Dickinson Biosciences, San Jose, CA). Unstained and single fluorochrome controls were used for background subtraction.

Clonogenic assay: HEK 293 cells were transfected with TDP-43 siRNA or a control siRNA, 24 h post transfection cells were trypsinized and splitted onto 60 mm plates. At 48 h post transfection cells were treated with IR (3 Gy) in the RS-2000 (RAD-Source). Cells were allowed to grow for 10 days and colonies were counted by staining with crystal violet.

NHEJ assay for the repair of DSBs

We employed two plasmid based approach to measure NHEJ-mediated DSB repair proficiency, namely, the standard I-SceI based GFP reporter assay and a shuttle plasmid containing an unligatable DSB termini, developed in our laboratory.

I-SceI based GFP reporter assay: For in cell NHEJ repair assays, SH-SY5Y cells were transfected with NHEJ reporter plasmid pimEJ5GFP, followed by selection with 10 μg/mL of Puromycin to establish stable integration line (52). The differentiated SH-SY5Y-EJ5GFP cells were then transfected with control or TDP-43 siRNA. At the time-point of 72 h post-transfection, I-SceI expression plasmid pCBASceI was transfected to both control and TDP-43 siRNA treated cells (53). After 12 h post-transfection, cells were trypsinized and subjected to FACS analysis using BD LSRII flow cytometer (54). In parallel, similar NHEJ reporter assay was performed in dividing HEK293 cells. As a control for NHEJ pathway, HEK293 cells were transfected with NHEJ reporter plasmid followed by treatment with DNA-PK inhibitor NU7441 (10 μM) for 2 h, prior to I-SceI expression plasmid insertion. GFP expression images were taken using EVOS fluorescence microscope before FACS analysis.

NHEJ reporter assay using a shuttle plasmid containing an unligatable DSB termini: In view of the fact that the I-SceI restriction activity mediated clean-ended DSB substrates may not recapitulate physiological, *in cell* DSBs, which invariably contain blocked termini, we designed a plasmid substrate containing DSB lesions with blocked termini (dirty ends) mimicking IR- or drug-induced DSBs. Briefly, a 51-mer duplex oligo containing an internal U•U, was ligated to a GFP plasmid (**pNB1-a**.; BamH1/EcoR1 sites). Treatment of the plasmid with BER enzymes Udg + Fpg creates a linearized plasmid with unligatable 3'P ends and its re-circularization via DSB repair in mammalian cells allows GFP expression, as the DSB is located in between promoter and GFP coding sequence. Hence, all GFP-positive cells will contain re-circularized plasmids on kan^r (kanamycin resistance) selection. *Hirt* supernatants from transfected cells were used to recover the repaired plasmids, which were then multiplied in *E. coli* for sequencing after PCR using primers outside the repair target. Because any linear DNA is degraded in WT *E. coli* and is poorly transcribed in mammalian cells, only DSB repair occurring in human cells/extracts will be scored**.** The plasmid re-circularization was analyzed in control vs. TDP-43 KD cells. For *in vitro* repair, the pNB-1 plasmid was incubated with nuclear extracts from control or TDP-43 KD cells, in Hepes buffer containing 1 mM ATP and the products were analyzed by 1% agarose gel electrophoresis as well as colony formation in *E. coli,* as before (1).

***C. elegans* DNA damage assay**

The DNA double-strand break repair assay was modified from Craig et al (55). In brief, stage matched young adult worms were irradiated for 10 min by a cesium-137 source at 390 rad/min for a total of 40 Gy. Irradiated worms were then allowed to lay eggs for 3-4 h on seeded nematode growth medium plates and the removed. Plates were scored 24 h later for numbers of dead eggs vs viable hatched larvae. Experiment 1, N=148 (N2) and 175 (*tdp-1/ok803)* from three replicate plates. Experiment 2, N=517 (N2) and 380 (*tdp-1/ok803)*) from five replicate plates. Progeny from non-irradiated control parent worms have >99% viability. Statistical analysis was performed using GraphPad Prism software. For etoposide experiments, synchronized arrested L1 worms were maintained in M9 buffer with etoposide (250 μM) for 24 h, washed 3-5 times, and either harvested immediately or allowed to recover for 24 h prior to harvest.

Total protein extraction from L1 stage *C. elegans*

Mixed populations of worms were processed by sodium hydroxide / hypochlorite treatment, as described earlier (56) to obtain stage-matched populations of embryos. L1 worms were arrested in M9 buffer in the absence of food and pelleted by centrifugation. The compressed pellets were resuspended in 2 volumes of lysis Buffer C (50 mM Tris–HCl, pH 7.4, 500 mM NaCl, 1 mM EDTA, 1 mM DTT, 0.5% Triton X-100, 20% glycerol, two mini-EDTA-free protease inhibitor tablets and phosphatase inhibitor cocktail 1X) (57) followed by 5-7 pulses of sonication at 6 amplitude for 10 s each on ice. The lysed nematodes extracts were

centrifuged at 13000 rpm for 10 min at 4 ºC. The clear lysates were separated and protein concentrations were measured by Bradford method.

Genomic DNA extraction from *C. elegans*

Both untreated and treated worms were washed 3-5 times in M9 buffer and pelleted by centrifugation at 1200 rpm for 4 min at room temperature, and snap-frozen in liquid nitrogen. The genomic DNA was extracted following the DNeasy Blood & Tissue Kit's protocol with minor modifications. The worm pellet was digested in 300 µl of ATL buffer with 50 µl proteinase K at 56 ºC, with intermittent pipetting, until the tissue is completely lysed. After that, 300 µl of buffer AL and 5 µl of RNAse A (50 mg/mL) were added to same tube, mixed well by pipetting and incubated at 56 ºC for another 15 min. Next, 400 µl of 100% ethanol were added to the same tube and mixed well by pipetting slowly for 4-5 times. The remainder of the extraction procedures were followed as described in the manufacturer's protocol.

Long Amplification PCR with *C. elegans* genomic DNA

Genomic DNA isolated from L1 stage N2 and *tdp-1(ok803)* worms were used to measure the extent of genome damage by long–amplification PCR (LA-PCR) method as described before. 30 ng of genomic DNA were used for vehicle treated, etoposide treated, and post-treatment recovery period nematode samples. Firstly, these DNA samples were run in 0.8% agarose gel along with 1 kb DNA ladder to check the DNA integrity in each sample. Next, the same amount of genomic DNA was used for amplification of 13.7 kb length of nuclear genomic region with a pair of primers NuF 13.7 / NuR 13.7 using LongAmp Taq polymerase in 25 µL reaction volume following the thermal cycling profile: 94 ºC for 2 min; 94 ºC for 30 sec, 60 ºC for 40 s, 65 ºC for 14 min (repeated for 25 cycles); 65 ºC for 15 min followed by cooling to 4ºC. The equal amounts of genomic DNA template were normalized by running a short amplification PCR reaction amplifying 225 bp nuclear genomic region using the primer pair NuF 225 / NuR 225 and RedTaq DNA polymerase enzyme following the thermal cycling conditions: 94 ºC for 2 min; 94 ºC for 30 s, 57 ºC for 30 s, 72 ºC for 30 s (repeated for 30 cycles); 72 ºC for 7 min and then cooling to 4 ºC. The relative band intensity of the long range amplicon of desired size reflected the extent of DNA damage in the respective samples measured by both running in agarose gel as well as quantitative estimation by dsDNA Picogreen quantitation method per the manufacturer's protocol (58, 59).

***In vitro* DSB repair assay in *C. elegans* extract**

DSB repair plasmid substrate was prepared by single digesting circular plasmid (~5.5 kb) with EcoRI, and was subsequently treated with shrimp alkaline phosphatase (SAP) to inhibit quick self-ligation. The efficiency of SAP treatment was monitored by transforming T4 Ligase-treated EcoRI digested plasmid into *E. coli* and counting bacterial colony number. For *in vitro* DSB repair assays 100 ng of plasmid substrates were incubated with 10µg of either N2 or CK501 nematodes protein extracts in repair assay buffer (50 mM Tris-HCl, pH 8.0, 5 mM $MgCl_2$, 50 mM NaCl, 20 mM KCl, 2 mM Aurin tricarboxylic Acid, 1mM DTT, 1 mM dNTP mix and 50 µg/mL BSA) in a 50 µL reaction volume at 30 ºC for 1 h. The reaction was stopped by adding 50 µL EDTA solution. Plasmid DNA was recovered by phenol: chloroform extraction method, and dissolved in nuclease free water. 5ng of DNA from each reaction were transformed in to E. coli strain XL10 Gold chemical competent cells and spreaded on agar plate with respective antibiotic selection. The number of bacterial colonies were counted after overnight incubation (1).

***In vitro* DSB plasmid re-circularization assay**

DSB carrying plasmid DNA substrate was prepared by digesting pLenti CMV GFP Blast (a gift from Eric Campeau & Paul Kaufman) with BamHI restriction enzyme cutting between CMV promoter and GFP coding sequence. The digested DNA was gel extracted using Qiagen Gel extraction kit following manufacturer's protocol. The DSB ligation efficiency was tested using (a) IP elution or (b) cell lysates, as below:

a)In this assay, endogenous XRCC4 IP was performed from control or TDP-43 siRNA transfected NP cells treated with etoposide (10 µM), using mouse IgG or anti-XRCC4 monoclonal antibody and Protein G

magnetic beads for 6 h at 4 ºC. Following IP, beads were sufficiently washed with washing buffer (1X TBS, 100 mM NaCl and 1X protease inhibitor). Finally, beads were resuspended in 1X PBS with 1X protease inhibitor and 1X phosphatase inhibitor cocktail. The 40 µl DSB assay reaction was composed of 100 ng of DSB plasmid substrate, 1X T4 ligation buffer (40 mM Tris-HCl (pH 8.0), 10 mM $MgCl_2$, 10 mM DTT, 10 mM ATP), 100 nM dNTP mix, 5 mM EDTA (pH 8.0), 10 µl of IP beads, 1X protease inhibitor and 1X phosphatase inhibitor, with or without 200 fmole of purified recombinant TDP-43. The assay was set up at 25 ºC for 30 min with continuous rotation. Next, 25 ng of unligated DSB plasmid substrate or 10 µl out of 40 µl reaction mix were transformed into *E. coli* XL-10 Gold competent cells and plated on agar plate with respective bacterial selection. Next day, number of bacterial colonies were counted in each plate. Colonies from unligated plasmid transformation were subtracted from number of colonies in experimental plates.

b) For assay with cell/tissue extracts, extracts were prepared in 1X RIPA buffer added with 1X protease inhibitor and 1X phosphatase inhibitor cocktail. For 40 µL ligation reaction, 100 ng of DSB plasmid substrate, 2X T4 ligation buffer (described above), 100 nM dNTP mix, 10 mM EDTA (pH 8.0), 10-15 µg of protein extract, 200 fmole of purified recombinant XRCC4/Lig4 complex supplement (in case of post-mortem/frozen tissue extracts). The reaction was set up at gently shaking condition at 25 ºC for 30 min, followed by transformation of 5 µl of the ligation reaction mix in to *E. coli* Xl-10 Gold competent cells. Ligation efficiency was measured by counting number of colonies on agar plate as before.

DNA Nick-ligation assay

DNA nick ligation assay was carried out with endogenous XRCC4 IP elution as described before (60). For the rescue assay, 200 fmole of purified TDP-43 was added to reaction mixture containing XRCC4 IP elution from TDP-43 KD cells.

Briefly, oligos for nicked duplex DNA substrate were custom synthesized by Sigma.

p24: 5′-Cy3-GGCACGGTCTACACGGCACACGAG -3′,

p27: 5′- TGTACATGATACGATTCCAAGCTAAGC -3′

p51: 5′- CCGTGCCAGATGTGCCGTGTGCTCACATGTACTATGCTAAGGTTCGATTCG -3′

Following the annealing of 10 pmol of each oligomer with 50 mM NaCl in boiling water, annealed oligomers were mixed with IP products with or without recombinant TDP-43 in 1X T4 ligation buffer and the mixture was incubated in a water bath for 10 min at 30 °C for ligation. Samples were then mixed with 2X TBE sample buffer, heated for 3 min at 100 °C, and subsequently cooled down on ice for 3 min before loading into denaturing urea polyacrylamide gel for electrophoresis. The band was detected by Typhoon FLA 7000 for Ligation Kinetic analysis.

Spinal cord total tissue extract preparation

Tissues were homogenized in RIPA buffer supplied with protease and phosphatase inhibitors (20 mM Tris-HCl, pH 7.5; 150 mM NaCl; 1 mM EDTA, 0.5 EGTA; 1% Sodium deoxycholate; 1% Triton-X-100 and 0.1% SDS). Tissue lysates were sonicated at 8 amplitude for 10 s for 6-7 times with 2 min interval between two consecutive pulses and followed by centrifugation at 13,000 rpm for 10 min at 4 ºC. The clear lysate was separated into another fresh tube, and centrifuged again at high speed to remove additional fat contaminations.

***In vitro* DSB plasmid re-circularization assay**

DSB carrying plasmid DNA substrate was prepared by digesting pLenti CMV GFP Blast (a gift from Eric Campeau & Paul Kaufman) with BamHI restriction enzyme cutting between CMV promoter and GFP coding sequence. The digested DNA was gel extracted using Qiagen Gel extraction kit following manufacturer's protocol. For assay with cell/tissue extracts, extracts were prepared in 1X RIPA buffer added with 1X protease inhibitor and 1X phosphatase inhibitor cocktail. For 40 µL ligation reaction, 100 ng of DSB plasmid substrate, 2X T4 ligation buffer (described above), 100 nM dNTP mix, 10 mM EDTA (pH 8.0), 10-15 µg of protein extract, 200 fmole of purified recombinant XRCC4/Lig4 complex supplement (in case of post-mortem/frozen tissue extracts). The reaction was set up at gently shaking condition at 25

ºC for 30 min, followed by transformation of 5 µl of the ligation reaction mix in to *E. coli* Xl-10 Gold competent cells. Ligation efficiency was measured by counting number of colonies on agar plate as before.

Immunohistochemistry of human tissue

5µm-thick formalin-fixed, paraffin-embedded sections were baked overnight at 60 °C, and deparaffinized and redydrated by subsequent changes with xylene and different dilutions of ethanol following rinsing with water for 5 min. After that, slides were boiled in 10mM sodium citrate buffer (pH 6.0) for 10 min and cooled on ice for 20 min. Endogenous peroxidase was quenched by treating with 3% hydrogen peroxide solution in methanol for 10 min at room temperature, followed by rinsing with double distilled water and 1X TBST for 5 min 3 changes. The processed sections were perfused with 0.2% Triton X-100 in PBS and then blocked with 2.5% horse serum for 30 min at room temperature. Afterwards, respective primary was diluted in Dako antibody diluent (polyclonal anti-TDP-43, 1:150 and monoclonal anti-γH2AX, 1:150) and applied for 1 h at room temperature in a moist chamber. After 3 washes in TBST for 5 min, the sections were incubated for 30 min with respective peroxidase-coupled secondary antibodies at room temperature in moist chamber. Washed again 3 times and developed with DAB-substrate chromogen mixture followed by rinsing 2 times with double distilled water. Each section was counterstained with Hematoxylin for 30-60 s, and rinsed with water. Then sections were dehydrated with ethanol and xylene, and mounted slides with coverslip.

Statistical analysis

Graphpad prism 6 or Microsoft excel software was used for data analysis. Comparisons of groups were generated with two-way Anova followed by Sidak's or Tukey's multiple comparison test to compare selected pair of means. *P*-values are indicated in the associated figure legends.

References

1. Dutta A*, et al.* (2017) Microhomology-mediated end joining is activated in irradiated human cells due to phosphorylation-dependent formation of the XRCC1 repair complex. *Nucleic Acids Res* 45(5):2585-2599.
2. Hirt B (1967) Selective extraction of polyoma DNA from infected mouse cell cultures. *J Mol Biol* 26(2):365-369.
3. Belanger M, Allaman I, & Magistretti PJ (2011) Brain energy metabolism: focus on astrocyte-neuron metabolic cooperation. *Cell Metab* 14(6):724-738.
4. Madabhushi R, Pan L, & Tsai LH (2014) DNA damage and its links to neurodegeneration. *Neuron* 83(2):266-282.
5. Madabhushi R*, et al.* (2015) Activity-Induced DNA Breaks Govern the Expression of Neuronal Early-Response Genes. *Cell* 161(7):1592-1605.
6. Schwer B*, et al.* (2016) Transcription-associated processes cause DNA double-strand breaks and translocations in neural stem/progenitor cells. *Proc Natl Acad Sci U S A* 113(8):2258-2263.
7. Suberbielle E*, et al.* (2013) Physiologic brain activity causes DNA double-strand breaks in neurons, with exacerbation by amyloid-beta. *Nat Neurosci* 16(5):613-621.
8. Suberbielle E*, et al.* (2013) Physiologic brain activity causes DNA double-strand breaks in neurons, with exacerbation by amyloid-[beta]. *Nat Neurosci* 16(5):613-621.
9. Sharma V*, et al.* (2016) Oxidative stress at low levels can induce clustered DNA lesions leading to NHEJ mediated mutations. *Oncotarget* 7(18):25377-25390.
10. Cannan WJ, Tsang BP, Wallace SS, & Pederson DS (2014) Nucleosomes suppress the formation of double-strand DNA breaks during attempted base excision repair of clustered oxidative damages. *J Biol Chem* 289(29):19881-19893.
11. Farg MA, Konopka A, Soo KY, Ito D, & Atkin JD (2017) The DNA damage response (DDR) is induced by the C9orf72 repeat expansion in amyotrophic lateral sclerosis. *Hum Mol Genet* 26(15):2882-2896.

12. Walker C*, et al.* (2017) C9orf72 expansion disrupts ATM-mediated chromosomal break repair. *Nat Neurosci* 20(9):1225-1235.
13. Wang H*, et al.* (2018) Mutant FUS causes DNA ligation defects to inhibit oxidative damage repair in Amyotrophic Lateral Sclerosis. *Nat Commun* 9(1):3683.
14. Tammaro M, Liao S, Beeharry N, & Yan H (2016) DNA double-strand breaks with 5' adducts are efficiently channeled to the DNA2-mediated resection pathway. *Nucleic Acids Res* 44(1):221-231.
15. Cortes Ledesma F, El Khamisy SF, Zuma MC, Osborn K, & Caldecott KW (2009) A human 5'-tyrosyl DNA phosphodiesterase that repairs topoisomerase-mediated DNA damage. *Nature* 461(7264):674-678.
16. Dellaire G, Kepkay R, & Bazett-Jones DP (2009) High resolution imaging of changes in the structure and spatial organization of chromatin, gamma-H2A.X and the MRN complex within etoposide-induced DNA repair foci. *Cell Cycle* 8(22):3750-3769.
17. Aparicio T, Baer R, Gottesman M, & Gautier J (2016) MRN, CtIP, and BRCA1 mediate repair of topoisomerase II-DNA adducts. *J Cell Biol* 212(4):399-408.
18. Shackelford DA (2006) DNA end joining activity is reduced in Alzheimer's disease. *Neurobiol Aging* 27(4):596-605.
19. Sepe S*, et al.* (2016) Inefficient DNA Repair Is an Aging-Related Modifier of Parkinson's Disease. *Cell Rep* 15(9):1866-1875.
20. Wang WY*, et al.* (2013) Interaction of FUS and HDAC1 regulates DNA damage response and repair in neurons. *Nat Neurosci* 16(10):1383-1391.
21. Constantinescu D, Csoka AB, Navara CS, & Schatten GP (2010) Defective DSB repair correlates with abnormal nuclear morphology and is improved with FTI treatment in Hutchinson-Gilford progeria syndrome fibroblasts. *Exp Cell Res* 316(17):2747-2759.
22. King A*, et al.* (2015) ALS-FUS pathology revisited: singleton FUS mutations and an unusual case with both a FUS and TARDBP mutation. *Acta Neuropathol Commun* 3:62.
23. Hegde ML*, et al.* (2016) Scaffold attachment factor A (SAF-A) and Ku temporally regulate repair of radiation-induced clustered genome lesions. *Oncotarget* 7(34):54430-54444.
24. Hegde ML*, et al.* (2012) Enhancement of NEIL1 protein-initiated oxidized DNA base excision repair by heterogeneous nuclear ribonucleoprotein U (hnRNP-U) via direct interaction. *J Biol Chem* 287(41):34202-34211.
25. Sui J*, et al.* (2015) DNA-PKcs phosphorylates hnRNP-A1 to facilitate the RPA-to-POT1 switch and telomere capping after replication. *Nucleic Acids Res* 43(12):5971-5983.
26. Haley B, Paunesku T, Protic M, & Woloschak GE (2009) Response of heterogeneous ribonuclear proteins (hnRNP) to ionising radiation and their involvement in DNA damage repair. *Int J Radiat Biol* 85(8):643-655.
27. Zhou B, Liu C, Geng Y, & Zhu G (2015) Topology of a G-quadruplex DNA formed by C9orf72 hexanucleotide repeats associated with ALS and FTD. *Sci Rep* 5:16673.
28. Beck J*, et al.* (2013) Large C9orf72 hexanucleotide repeat expansions are seen in multiple neurodegenerative syndromes and are more frequent than expected in the UK population. *Am J Hum Genet* 92(3):345-353.
29. Storici F, Bebenek K, Kunkel TA, Gordenin DA, & Resnick MA (2007) RNA-templated DNA repair. *Nature* 447(7142):338-341.
30. Wei W*, et al.* (2012) A role for small RNAs in DNA double-strand break repair. *Cell* 149(1):101-112.
31. Hegde ML*, et al.* (2010) Specific Inhibition of NEIL-initiated repair of oxidized base damage in human genome by copper and iron: potential etiological linkage to neurodegenerative diseases. *J Biol Chem* 285(37):28812-28825.
32. Encinas M*, et al.* (2000) Sequential treatment of SH-SY5Y cells with retinoic acid and brain-derived neurotrophic factor gives rise to fully differentiated, neurotrophic factor-dependent, human neuron-like cells. *J Neurochem* 75(3):991-1003.

33. Lander ES, *et al.* (2001) Initial sequencing and analysis of the human genome. *Nature* 409(6822):860-921.
34. Jordan PM, *et al.* (2009) Generation of spinal motor neurons from human fetal brain-derived neural stem cells: role of basic fibroblast growth factor. *J Neurosci Res* 87(2):318-332.
35. Du ZW, *et al.* (2015) Generation and expansion of highly pure motor neuron progenitors from human pluripotent stem cells. *Nat Commun* 6:6626.
36. Vasquez V, *et al.* (2017) Chromatin-Bound Oxidized alpha-Synuclein Causes Strand Breaks in Neuronal Genomes in in vitro Models of Parkinson's Disease. *J Alzheimers Dis*.
37. Freibaum BD, Chitta RK, High AA, & Taylor JP (2010) Global analysis of TDP-43 interacting proteins reveals strong association with RNA splicing and translation machinery. *J Proteome Res* 9(2):1104-1120.
38. Wang T, Wei JJ, Sabatini DM, & Lander ES (2014) Genetic screens in human cells using the CRISPR-Cas9 system. *Science* 343(6166):80-84.
39. Hegde PM, *et al.* (2015) The C-terminal Domain (CTD) of Human DNA Glycosylase NEIL1 Is Required for Forming BERosome Repair Complex with DNA Replication Proteins at the Replicating Genome: DOMINANT NEGATIVE FUNCTION OF THE CTD. *J Biol Chem* 290(34):20919-20933.
40. Yang C, *et al.* (2017) Regulation of oxidized base damage repair by chromatin assembly factor 1 subunit A. *Nucleic Acids Res* 45(2):739-748.
41. Leduc F, *et al.* (2011) Genome-wide mapping of DNA strand breaks. *PLoS One* 6(2):e17353.
42. Capp JP, *et al.* (2006) The DNA polymerase lambda is required for the repair of non-compatible DNA double strand breaks by NHEJ in mammalian cells. *Nucleic Acids Res* 34(10):2998-3007.
43. Dou H, *et al.* (2008) Interaction of the human DNA glycosylase NEIL1 with proliferating cell nuclear antigen. The potential for replication-associated repair of oxidized bases in mammalian genomes. *J Biol Chem* 283(6):3130-3140.
44. Hegde ML, *et al.* (2008) Physical and functional interaction between human oxidized base-specific DNA glycosylase NEIL1 and flap endonuclease 1. *J Biol Chem* 283(40):27028-27037.
45. Vasquez V, *et al.* (2017) Chromatin-Bound Oxidized alpha-Synuclein Causes Strand Breaks in Neuronal Genomes in in vitro Models of Parkinson's Disease. *J Alzheimers Dis* 60(s1):S133-S150.
46. Hegde ML, *et al.* (2013) Prereplicative repair of oxidized bases in the human genome is mediated by NEIL1 DNA glycosylase together with replication proteins. *Proc Natl Acad Sci U S A* 110(33):E3090-3099.
47. Wei L, *et al.* (2008) Rapid recruitment of BRCA1 to DNA double-strand breaks is dependent on its association with Ku80. *Mol Cell Biol* 28(24):7380-7393.
48. Kovalenko OA & Santos JH (2009) Analysis of oxidative damage by gene-specific quantitative PCR. *Curr Protoc Hum Genet* Chapter 19:Unit 19 11.
49. Sarker AH, *et al.* (2014) NEIL2 protects against oxidative DNA damage induced by sidestream smoke in human cells. *PLoS One* 9(3):e90261.
50. Chakraborty A, *et al.* (2015) Neil2-null Mice Accumulate Oxidized DNA Bases in the Transcriptionally Active Sequences of the Genome and Are Susceptible to Innate Inflammation. *J Biol Chem* 290(41):24636-24648.
51. Pandey A, *et al.* (2015) Berberine and Curcumin Target Survivin and STAT3 in Gastric Cancer Cells and Synergize Actions of Standard Chemotherapeutic 5-Fluorouracil. *Nutr Cancer* 67(8):1293-1304.
52. Bennardo N, Cheng A, Huang N, & Stark JM (2008) Alternative-NHEJ is a mechanistically distinct pathway of mammalian chromosome break repair. *PLoS Genet* 4(6):e1000110.
53. Richardson C, Moynahan ME, & Jasin M (1998) Double-strand break repair by interchromosomal recombination: suppression of chromosomal translocations. *Genes Dev* 12(24):3831-3842.

54. Liu J*, et al.* (2012) Protein phosphatase PP4 is involved in NHEJ-mediated repair of DNA double-strand breaks. *Cell Cycle* 11(14):2643-2649.
55. Craig AL, Moser SC, Bailly AP, & Gartner A (2012) Methods for studying the DNA damage response in the Caenorhabdatis elegans germ line. *Methods Cell Biol* 107:321-352.
56. Emmons SW, Klass MR, & Hirsh D (1979) Analysis of the constancy of DNA sequences during development and evolution of the nematode Caenorhabditis elegans. *Proc Natl Acad Sci U S A* 76(3):1333-1337.
57. Asagoshi K*, et al.* (2012) Single-nucleotide base excision repair DNA polymerase activity in C. elegans in the absence of DNA polymerase beta. *Nucleic Acids Res* 40(2):670-681.
58. Hunter SE, Jung D, Di Giulio RT, & Meyer JN (2010) The QPCR assay for analysis of mitochondrial DNA damage, repair, and relative copy number. *Methods* 51(4):444-451.
59. Gonzalez-Hunt CP*, et al.* (2016) PCR-Based Analysis of Mitochondrial DNA Copy Number, Mitochondrial DNA Damage, and Nuclear DNA Damage. *Curr Protoc Toxicol* 67:20 11 21-20 11 25.
60. Della-Maria J*, et al.* (2012) The interaction between polynucleotide kinase phosphatase and the DNA repair protein XRCC1 is critical for repair of DNA alkylation damage and stable association at DNA damage sites. *J Biol Chem* 287(46):39233-39244.

Supplementary Table S1. Clinical features of ALS patients and matched controls.

ALS patients from VA Biorepository Brain Bank					
	Case #	Age	Gender	Ethnicity	PMI (cr)[b] (hours)
Control	090015	66	M	Hispanic/Latino	<4.0
	100012	81	F	White	<4.0
	110005	62	M	Hispanic/Latino	2.75
	110006	68	M	White	1.5
ALS	100031	76	M	White	3.25
	100034	62	M	African American	1.66
	100039	50	M	White	5.0
	110007	80	M	White	1.25
	110009	84	M	White	3.58
	110011	83	M	White	2.5
	110036	85	M	White	2.5
	120011	58	F	White	1.0
	120018	83	M	African American	0.25
	120021	70	M	White	0.5
Guam-ALS patient samples					
	Case #	Age	Gender	Ethnicity	PMI (cr)[b] (hours)
Control	9311	57	F	Pacific Islander	1
	93855	43	F	Pacific Islander	16
	93842	48	M	Pacific Islander	15
	93869	49	M	Pacific Islander	25
	93866	63	M	Pacific Islander	13.5
ALS-Guam	93882	45	M	Pacific Islander	5
	9314	54	F	Pacific Islander	18.5
	93749	34	F	Pacific Islander	3.5
	93912	47	F	Pacific Islander	3
	9362	59	M	Pacific Islander	7

Supplementary Table S2. Clinical features of ALS patients and matched controls.

VA Biorepository Brain Bank		
	Case #	Cause of Death
Control	090015	1. Immediate COD: severe, acute abscessing bronchopneumonia (culture positive for Klebsiella pneumoniae and Pseudomonas aeruginosa). 2. Underlying COD: post-surgical repair of gastric ulcer.
	100012	1. Likely immediate COD: early, diffuse alveolar damage (DAD) of the lungs. 2. Intermediate COD: sepsis. Microbiologic cultures performed at the time of autopsy negative for any bacterial or fungal organisms in the blood. Signs and symptoms consistent with sepsis including shock, cardiopulmonary failure, renal insufficiency, metabolic acidosis and coagulopathy. Treated aggressively with antibiotic therapy. 3. Underlying COD: acute colitis.. Both infectious and ischemic etiologies of the colon.
	110005	1. Immediate COD: pulmonary edema due to cardiopulmonary dysfunction. 2. Underlying COD: severe coronary artery disease and hypertensive cardiomyopathy. 3. Past history significant for hypertension, hyperlipidemia, peripheral vascular disease, diabetes type II, and coronary artery disease.
	110006	1. Immediate COD: broncho-pneumonia and pleuritic. 2. Underlying COD: T-cell lymphoproliferative disorder consistent with T-cell lymphoma, not otherwise specified. 3. Acute renal tubular injury, most likely secondary to bronchopneumonia. 4. History of asbestosis and COPD
ALS	100031	1. ALS (rapid onset, progression). 2. Respiratory insufficiency
	100034	1. Heart failure. 2. Respiratory failure. 3. ALS.
	100039	1. Respiratory failure.
	110007	1. ALS primary 2. Intercostal Respiratory failure (secondary).
	110009	1. ALS complications.
	110011	1. ALS.
	110036	1. ALS.
	120011	1. ALS.
	120018	1. ALS.
	120021	1. Respiratory failure due to ALS.

Supplementary Table S3. Lists the antibodies used in this study. WB: Western blot; IF: Immunofluorescence; IP: immunoprecipitation.

Antibody	Species	Application			Ref: / Suppliers	
		WB	IF	IP	Suppliers	Cat #
TDP-43	rabbit	1:1000	1:100		Protein Tech	10782-2-AP
TDP-43	mouse	1:1000	1:200	1:1000	R&D Systems	MAB7778
SOX2	mouse	1:1000	1:100		R&D Systems	AF2018
GAPDH	mouse	1:2000			Protein Tech	6004-1-IG
XRCC4	rabbit		1:50		Abcam	ab118008
Ligase IV	rabbit		1:50		Abcam	ab80514
XRCC1	rabbit	1:1000			Abcam	ab134056
Ligase III	rabbit	1:1000			Abcam	ab185815
ATM	rabbit	1:800			Abcam	ab32420
p-ATM (S1981)	rabbit	1:600	1:50		Abcam	ab81292
Biotin	rabbit			1:1000	Abcam	ab53494
Ubiquitin	rabbit	1:250			Abcam	ab7780
Apoptosis Cocktail		1:100			Abcam	ab136812
Histone 3	rabbit	1:1000			Cell Signaling	4499
Beta-actin	mouse	1:2500			Cell Signaling	3700
DNA-PKcs (3H6)	mouse	1:1000	1:50		Cell Signaling	12311
53BP1	rabbit	1:750	1:50	1:500	Cell Signaling	4937
p-53BP1 (S1778)	rabbit	1:750	1:50		Cell Signaling	2675
p-H2AX (S139)	rabbit	1:1000	1:100		Cell Signaling	9718
Cleaved-PARP1	rabbit	1:1000			Cell Signaling	5625
Cleaved Caspase-3	rabbit	1:750			Cell Signaling	9661
Normal Rab IgG				1:1000	Cell Signaling	2729
Pol lambda	rabbit	1:500	1:50		Thermo Fisher	AA526937
Hb9	rabbit		1:50		Thermo Fisher	PA5-23407
Texas Red-X	mouse		1:1000		Thermo Fisher	T-862
Alexa Fluor® 488	rabbit		1:1000		Thermo Fisher	A-11008
Pol Mu	rabbit	1:800			GeneTex	GTX116332
βIII Tubulin	mouse		1:100		GeneTex	GTX631836
MAP2	mouse		1:100		GeneTex	GTX11267
Nestin	mouse	1:1000	1:100		GeneTex	GTX30671
Oct 3/4	rabbit	1:600			GeneTex	GTX101497
p-H2AX (S139)	mouse	1:1000		1:1000	EMD Millipore	05-636
Isl-1	rabbit		1:300		EMD Millipore	AB4326
FLAG-M2-HRP	mouse	1:1500			Sigma	A8592
Ku70	mouse	1:500	1:40		Abnova	H00002541MOI
Normal Ms IgG				1:1000	Santa Cruz	sc-2025
XRCC4 (C-4)	mouse	1:500		1:200	Santa Cruz	sc-271087
Ligase IV (D-8)	mouse	1:500			Santa Cruz	sc-271299
XLF (D-1)	mouse	1:500			Santa Cruz	sc-166488

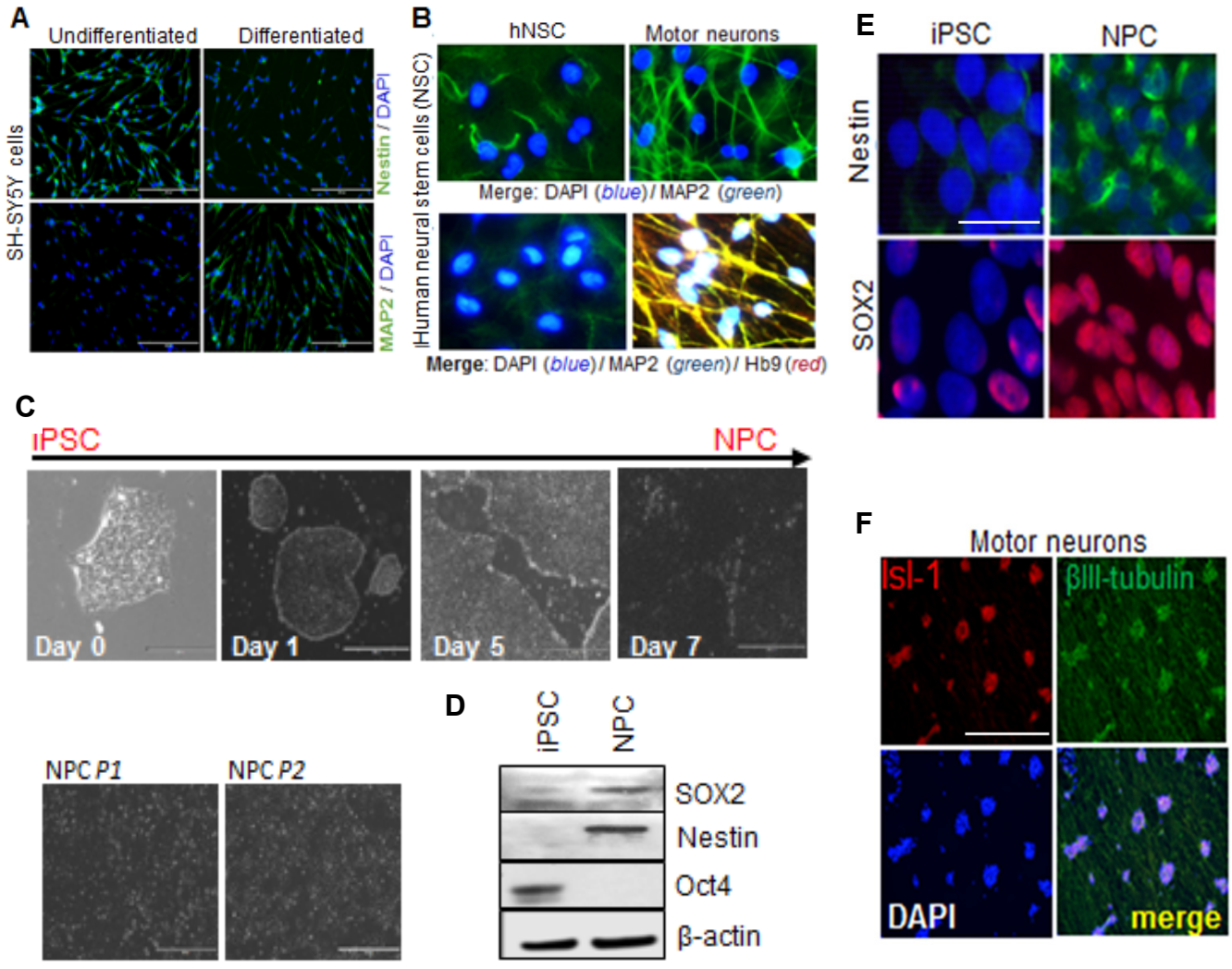

Fig. S1. Neuronal differentiation optimization and characterization by motor neuron markers. (Related to Fig. 1.) (*A*, *Left*) Undifferentiated SH-SY5Y cells (left) and their neuronal differentiation (right). Immunofluorescence with neuronal markers anti-Nestin or anti-MAP2 antibody. The nuclei were counterstained with DAPI. (Scale bars: 200μm.) (*B*, *Right*) Undifferentiated Human neural stem cells (NSC) (left) and differentiated motor neurons (right). Immunofluorescence with neuronal marker anti-MAP2 antibody and motor neuron marker anti-Hb9 antibody. The nuclei were counterstained with DAPI. (Scale bars: 100μm.) (*C*) Representative image of induction of pluripotent stem cells (iPSC) into neural progenitor cells (NPC). (Scale bars: 400μm.) (*D*) Immunoblotting (IB) of total cell lysates from iPSC and NPC with stem cell marker anti-Oct 4 and neural precursor markers anti-Nestin and anti-SOX2 antibody. (*E*) Immunofluorescence with neural progenitor markers anti-Nestin and anti-SOX2 antibody. (Scale bars: 40μm.) (*F*) Immunofluorescence of NPC-derived motor Neurons with motor neuron markers anti-Isl-1 or anti-βIII-tubulin antibody. (Scale bars: 200μm.)

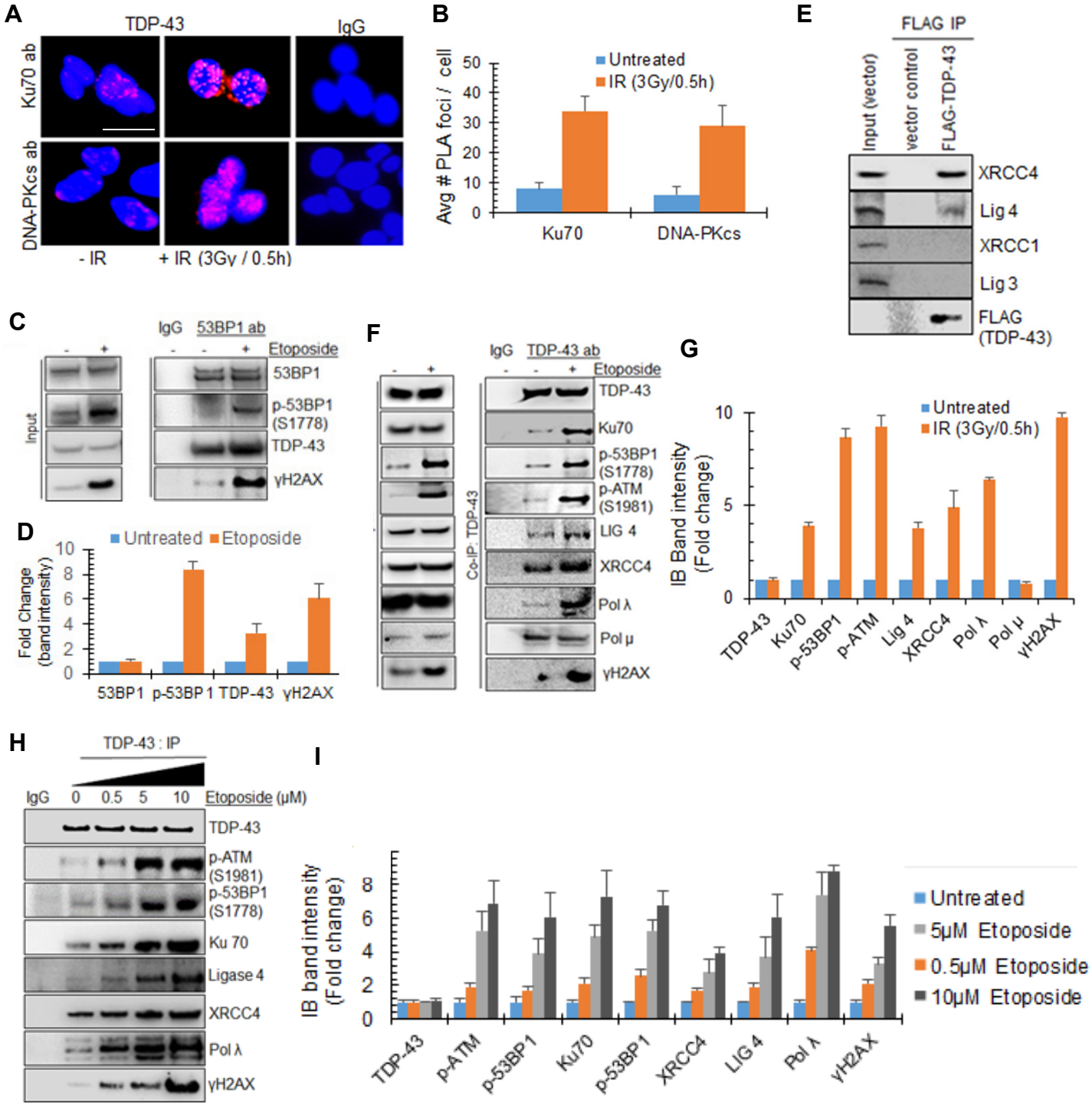
A
TDP-43
IgG
Ku70 ab
DNA-PKcs ab
- IR
+ IR (3Gy / 0.5h)
B
Untreated
IR (3Gy/0.5h)
Avg # PLA foci / cell
Ku70
DNA-PKcs
E
FLAG IP
Input (vector)
vector control
FLAG-TDP-43
XRCC4
Lig 4
XRCC1
Lig 3
FLAG (TDP-43)
C
IgG
53BP1 ab
Etoposide
Input
53BP1
p-53BP1 (S1778)
TDP-43
γH2AX
D
Untreated
Etoposide
Fold Change (band intensity)
53BP1
p-53BP1
TDP-43
γH2AX
F
IgG
TDP-43 ab
Etoposide
Co-IP: TDP-43
TDP-43
Ku70
p-53BP1 (S1778)
p-ATM (S1981)
LIG 4
XRCC4
Pol λ
Pol μ
γH2AX
G
Untreated
IR (3Gy/0.5h)
IB Band intensity (Fold change)
TDP-43
Ku70
p-53BP1
p-ATM
Lig 4
XRCC4
Pol λ
Pol μ
γH2AX
H
TDP-43 : IP
IgG
0
0.5
5
10
Etoposide (μM)
TDP-43
p-ATM (S1981)
p-53BP1 (S1778)
Ku 70
Ligase 4
XRCC4
Pol λ
γH2AX
I
IB band intensity (Fold change)
Untreated
5μM Etoposide
0.5μM Etoposide
10μM Etoposide
TDP-43
p-ATM
p-53BP1
Ku70
p-53BP1
XRCC4
LIG 4
Pol λ
γH2AX

Fig. S2. TDP-43 specifically interacts with NHEJ proteins. (Related to Fig. 1.). (*A* and *B*) NPCs were treated with irradiation with 3Gy dose and cells were fixed 30mins post-IR for proximity ligation assay (PLA) pairwise between anti-TDP-43 vs control IgG or anti-Ku70 or anti-DNA-PKcs antibody. Quantitation of average PLA foci per cell (N= 25-30 cells). (Scale bars: 20μm.) Data are presented as means ± s.d. (*C* and *D*) Endogenous 53BP-1 IP using anti-53BP1 antibody (Rabbit) from Etoposide-treated NPC total cell extracts. IP with IgG (Rabbit) served a s control. Histogram shows quantitation of IB band intensity. (*E)* Neural progenitor cells (NPC) transfected with vector control or plasmid expressing FLAG-TDP-43. Total cell lysates were subjected to IP with anti-FLAG antibody, then immunoblotted with anti-XRCC4, anti-Lig4, anti-XRCC1, anti-Lig3 and anti-FLAG antibody. (*F* and *G*) differentiated SH-SY5Y cells were treated with 10μM Etoposide or vehicle for 4h. Chromatin extracts from treated and untreated cells were subjected to immunoprecipitation (IP) with control IgG (mouse) or anti-TDP-43 antibody, (*F*) immunoprecipitates were then probed with anti-TDP-43, anti-Ku70, anti-p53BP1(S1778), anti-pATM(S1981), anti-Lig4, anti-XRCC4, anti-polλ, anti-polμ and anti-H2AX(S139), (*G*) relative IB band intensity quantitation. (*H* and *I*) Endogenous TDP-43 IP from Etoposide-treated NPCs shows dose-dependent association of TDP-43 with NHEJ (XRCC4, Lig4 and polλ) and DDR (pATM S1981, p53BP1 S1778, Ku70 and γH2AX) factors.

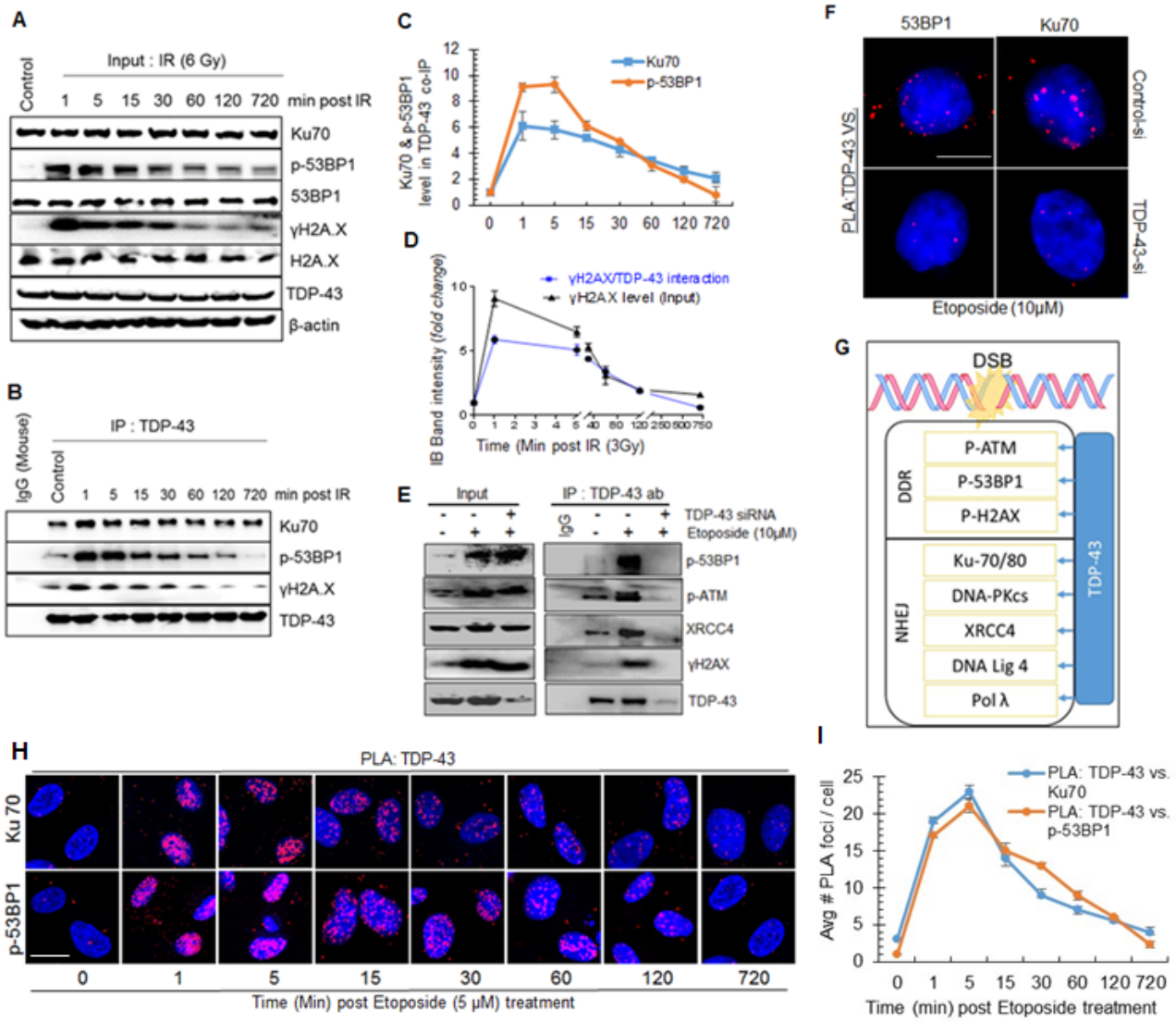

Fig. S3. Kinetics of TDP-43's interaction with DNA damage/repair proteins after damage induction. (Related to Fig. 1.). (*A-D*) Differentiated SH-SY5Y cells were subjected to IR with 6Gy dose and harvested at the indicated time-points. Total nuclear lysates from untreated or treated samples were subjected to IP with control IgG or anti-TDP-43 antibody, then immunoprecipitates and respective input samples were probed with anti-Ku70, anti-p53BP1(S1778), anti-53BP1, anti-pH2AX(S139), anti-H2AX, anti-TDP-43 and anti-β-actin antibody (*A* and *B*), quantitation of band intensity (*C*), (*D*) quantitation of TDP-43 vs γH2AX interaction kinetics following IR treatment. (*E* and *F*) Validation of anti-TDP-43 antibody. SH-SY5Y cells were transfected with either control or TDP-43 antisense RNA, followed by Etoposide treatment. Total cell lysates were subjected to IP with control IgG or anti-TDP-43 antibody, then probed with anti-p53BP1, anti-pATM, anti-XRCC4, anti-γH2AX and anti-TDP-43 antibody (*E*). (*F*) NP cells were similarly transfected with control or TDP-43 siRNA and treated with Etoposide, then PLA was performed with anti-TDP-43 vs anti-53BP1 or anti-Ku70 antibody. (Scale bars: 20μm.) (*G*) Schematic list of DNA DSB repair and response factors interacting with TDP-43. Data are presented as means ± s.d. (*H* and *I*) Time kinetics of TDP-43's association with NHEJ factors analyzed by PLA. NSC-derived motor neurons were treated with Etoposide (5μM, 4h) and subjected to PLA analysis at indicated time-points (*H*). Quantitation of average number of PLA foci from >25 cells at each time point (*I*)**.** Scale bars: 10μm. All values are from three independent experiments ± s.d.

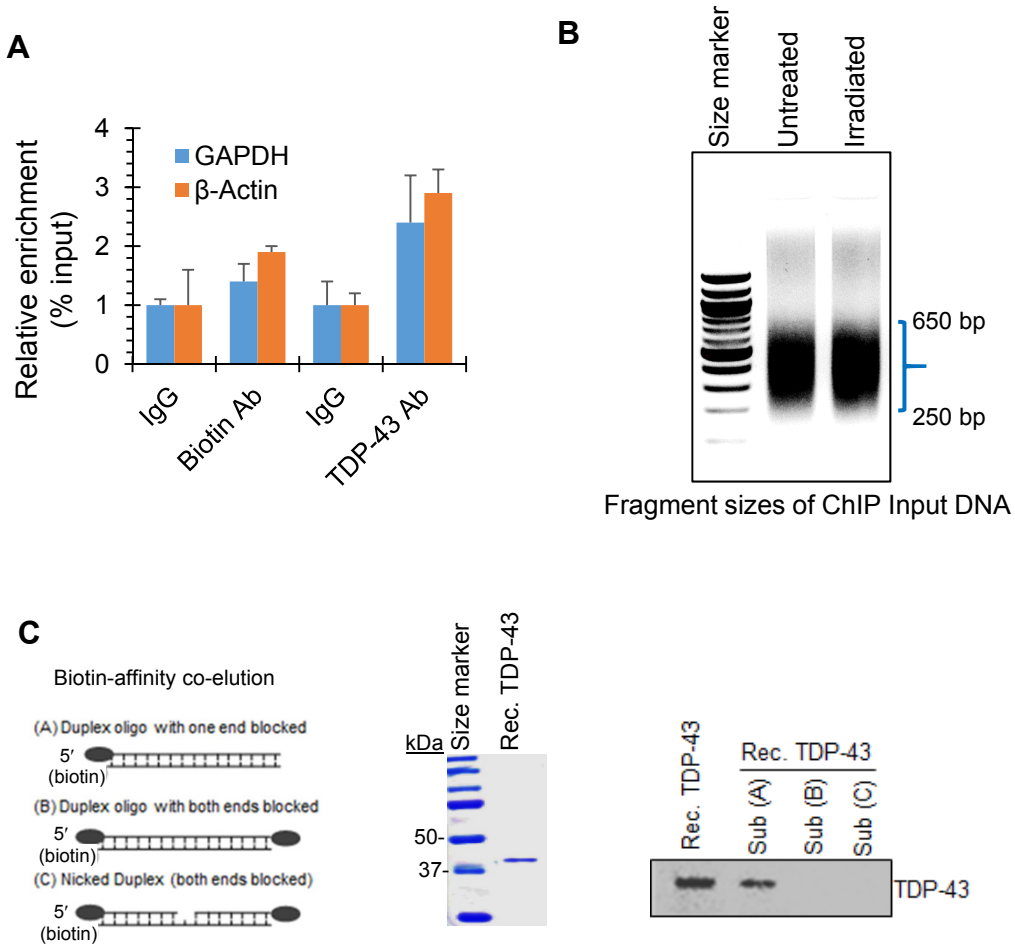

Fig. S4. TDP-43 binds to double-strand break sites in the genome. (Related to Fig. 2.). (*A*) Real time PCR based quantitation of Re-ChIP assay. First ChIP using anti-Biotin antibody followed by Re-ChIP with anti-TDP-43 antibody in untreated cells targeting selected regions of *GAPDH* and β-*actin* genes. (*B*) Representative image of agarose gel separation of the input DNA fragment size between 250bp and 650bp used in dDIP/ChIP assay. Data are presented as means ± s.d. (*C*) *In vitro* binding of recombinant TDP-43 to a synthetic duplex oligo biotinylated at one or both termini, mimicking DSB, SSB, or intact duplex using affinity co-elution analysis (*Left*), SDS-PAGE image for purified recombinant TDP-43 (*Middle*), and IB of biotin co-elutes for anti-TDP-43 antibody (*Right*).

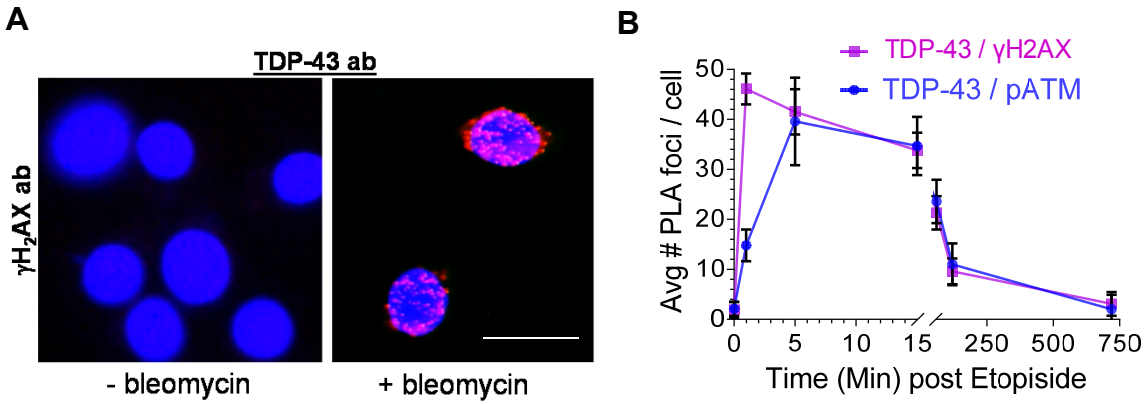

Fig. S5. TDP-43 directly interacts with γH2AX after bleomycin treatment in NPC**.** (Related to Fig. 2.). (*A*) PLA foci of anti-TDP-43 vs. anti-γH2AX antibody with or without bleomycin treatment in NP cells. (Scale bars: 20 μm.). (*B*) Time kinetics (0-12.5h) of PLA foci quantitation for anti-TDP-43 vs. anti-γH2AX or anti-p-ATM post Etoposide (5μM) treatment in NP cells. Data are presented as means ± s.d.

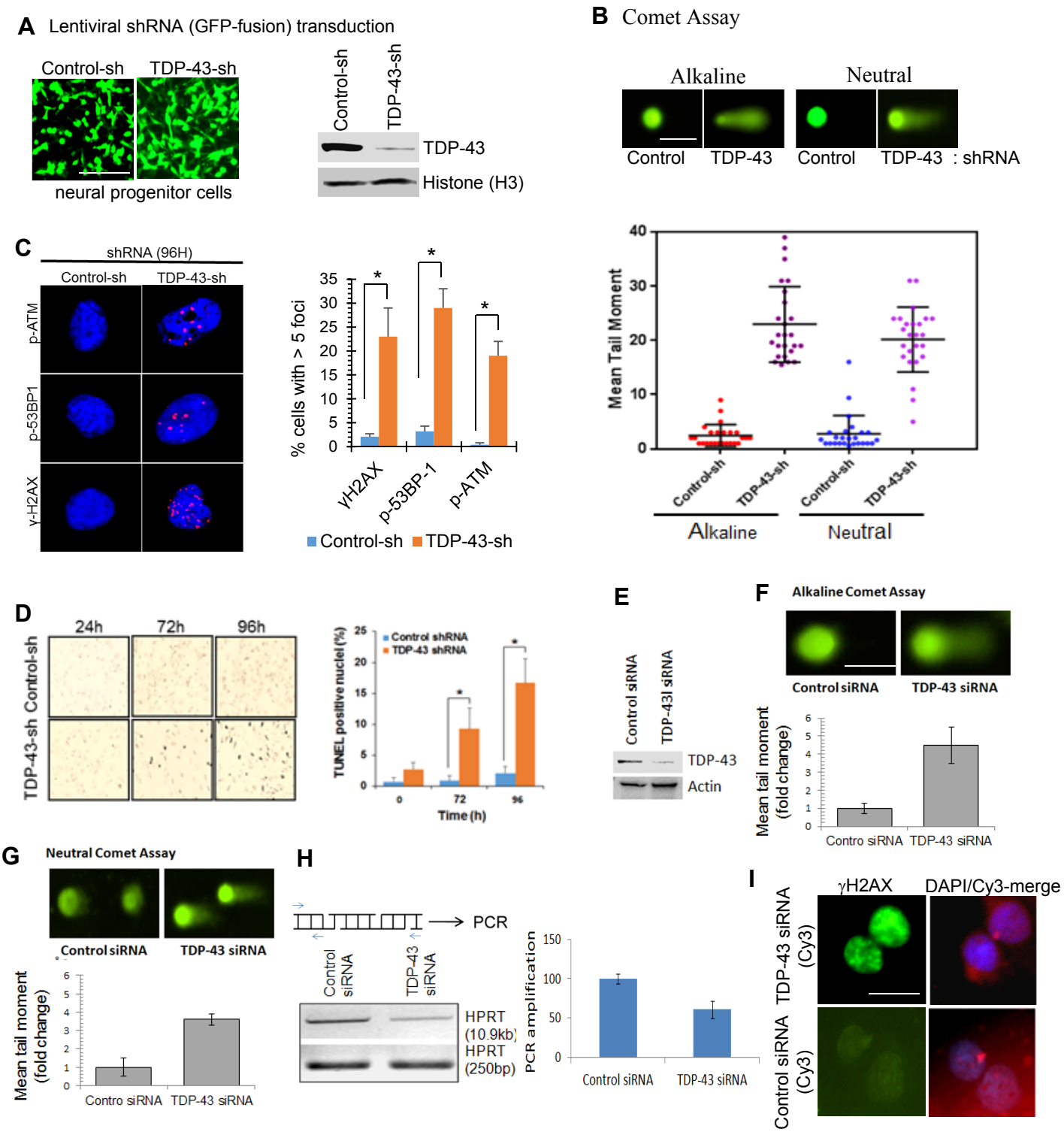
A
Lentiviral shRNA (GFP-fusion) transduction
Control-sh
TDP-43-sh
neural progenitor cells
Control-sh
TDP-43-sh
TDP-43
Histone (H3)
B
Comet Assay
Alkaline
Neutral
Control
TDP-43
Control
TDP-43 : shRNA
C
shRNA (96H)
Control-sh
TDP-43-sh
p-ATM
p-53BP1
γ-H2AX
% cells with > 5 foci
γH2AX
p-53BP-1
p-ATM
Control-sh
TDP-43-sh
Mean Tail Moment
Control-sh
TDP-43-sh
Control-sh
TDP-43-sh
Alkaline
Neutral
D
24h
72h
96h
TDP-43-sh
Control-sh
TUNEL positive nuclei (%)
Control shRNA
TDP-43 shRNA
Time (h)
E
Control siRNA
TDP-43l siRNA
TDP-43
Actin
F
Alkaline Comet Assay
Control siRNA
TDP-43 siRNA
Mean tail moment (fold change)
Contro siRNA
TDP-43 siRNA
G
Neutral Comet Assay
Control siRNA
TDP-43 siRNA
Mean tail moment (fold change)
Contro siRNA
TDP-43 siRNA
H
PCR
Control siRNA
TDP-43 siRNA
HPRT (10.9kb)
HPRT (250bp)
PCR amplification
Control siRNA
TDP-43 siRNA
I
γH2AX
DAPI/Cy3-merge
TDP-43 siRNA (Cy3)
Control siRNA (Cy3)

Fig. S6. TDP-43 depletion induces DNA damage accumulation and apoptosis in neuronal cells. (Related to Fig. 3.). (*A-D*) TDP-43 depletion using shRNA correlates to DSB accumulation in motor neurons genome. NPC-derived motor neurons were transduced with indicated lentiviral TDP-43 shRNA (GFP-tagged) constructs and were analyzed 96h post-transduction to achieve ~80% KD of TDP-43. (*A*) Representative IF image for control and TDP-43 shRNA tagged GFP expression (*Left*), immunoblotting of total cell lysates with anti-TDP-43 and anti-histone H3 antibody (*Right*). (Scale bars: 200μm.). (*B*) Alkaline (for total amount of DNA breaks) and Neutral (only for DSBs) comet assays in control or TDP-43 KD motor neurons indicating presence of ~4-6-fold higher DSBs (*Top*). (Scale bars: 10 μm.). Quantitation of mean comet tail moment from >25 cells (*Bottom*). *, $p<0.01$. (*C*) IF of TDP-43 KD motor neurons with anti-γH2AX, anti-p53BP1, and p-ATM antibody (*Left*), (Scale bars: 10μm.). Quantitation of cells with >5 IF foci (*Right*). *, $p<0.01$. (*D*) TUNEL analysis for estimation of DNA fragmentation in motor neurons transduced with indicated plasmids at 24, 72, and 96h time-points (Left). Quantitation of mean TUNEL-positive cells per field (Right). *, $p<0.01$. Data are expressed as mean ± SEM. (*E-I*) Differentiated SH-SY5Y cells were transfected with either control or TDP-43 siRNA, after 72h cells were collected for immunoblotting (IB), single cell electrophoresis (Comet) assay and long amplification PCR assay. (*E*) IB of total protein extracts probed with anti-TDP-43 and anti-actin antibody. (*F*) Alkaline comet assay estimating total DNA damage by measuring fold change of Comet tail moment. (Scale bars: 10μm.). (*G*) Neutral comet assay for double-strand break estimation in DNA, measured by Comet tail moment. (Scale bars: 40 μm.). (*H*) LA-PCR analysis from genomic DNA of treated and untreated cells by amplifying 10.9Kb region on *HPRT* gene, histogram shows picogreen quantitation of PCR product. (*I*) IF of γH2AX (green) in neural progenitor cells transfected with control or TDP-43 siRNA tagged with Cy3 (red). The green foci in red stained TDP-43 siRNA but not control siRNA transfected cells confirm DNA damage after TDP-43 KD. (Scale bars: 20μm.).

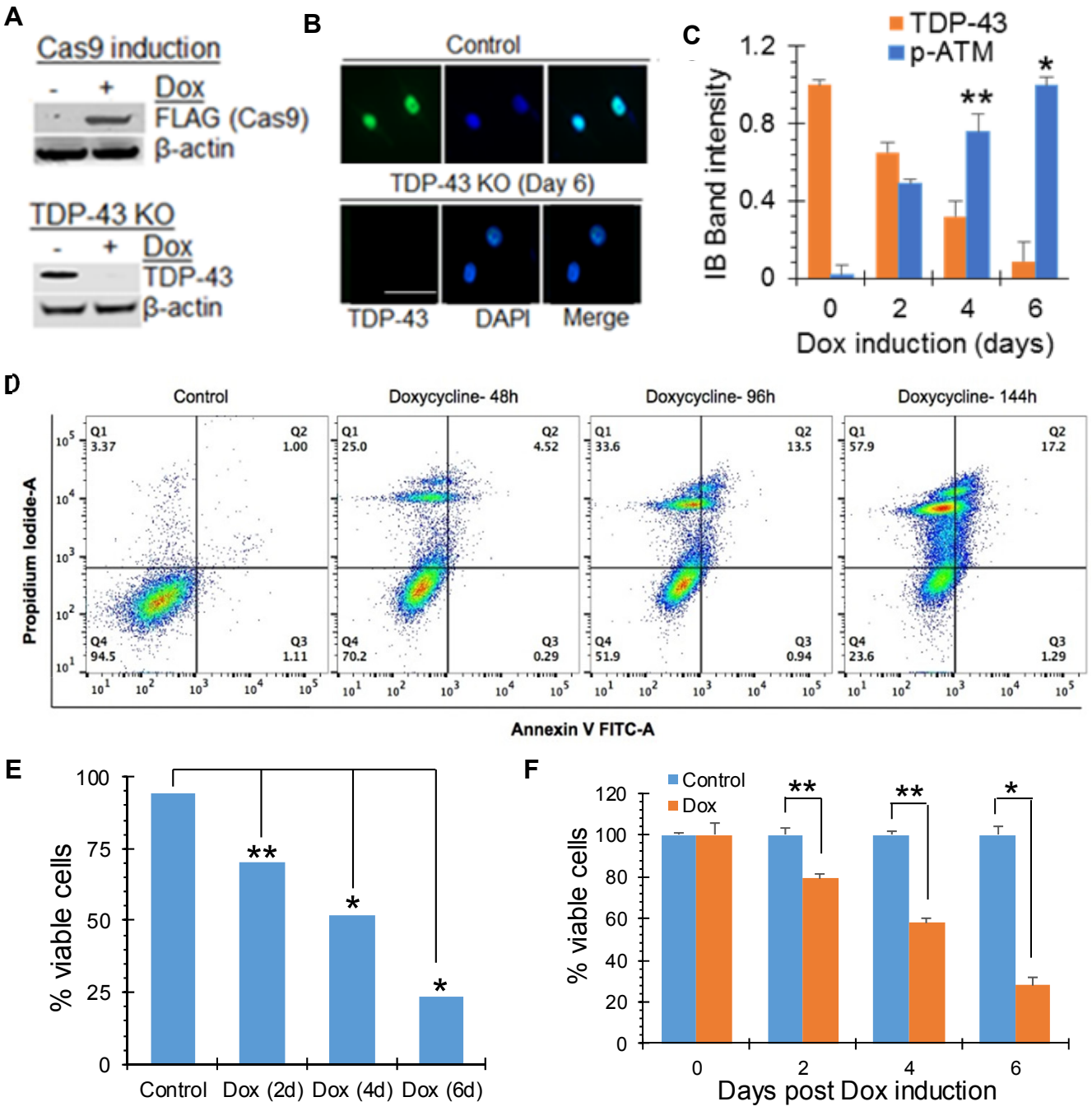

Fig. S7. TDP-43 depletion by conditional CRISPR/Cas9 induces DNA damage and apoptosis in neuronal cells (Related to Fig. 3.). (*A*) Immunoblotting with total cell lysates from conditional TDP-43 CRISPR/Cas9 KO cell line for Cas9 expression and TDP-43 KO with anti-FLAG or anti-TDP-43 and loading control anti-β-actin antibody. (*B*) IF with anti-TDP-43 antibody at 0 and 6 days post doxycycline induction. Nuclei were stained with DAPI. (Scale bars: 20µm.). (*C*) Quantitation of IB band intensity related to Fig. 3*B* of TDP-43 and p-ATM after Cas9 induction from three independent experiments. *, $p<0.01$; **, $p<0.05$. (*D* and *E*) Conditional TDP-43 CRISPR/Cas9 KO SH-SY5Y cells were double-stained with Annexin V/PI at 0, 2, 4 and 6 days post Dox induction of Cas9 and analyzed by flow cytometry. Results are presented in histogram as percentage of total apoptotic cells (early apoptotic (Q3)+ late apoptotic (Q2)). Error bars represent the ±SEM from N=3 independent experiments. (*F*) MTT assay for measuring cell viability after TDP-43 CRISPR/Cas9 KO in SH-SY5Y cells. *, $p<0.01$; **, $p<0.05$. Data are presented as means ± s.d. P values are based on two-way ANOVA.

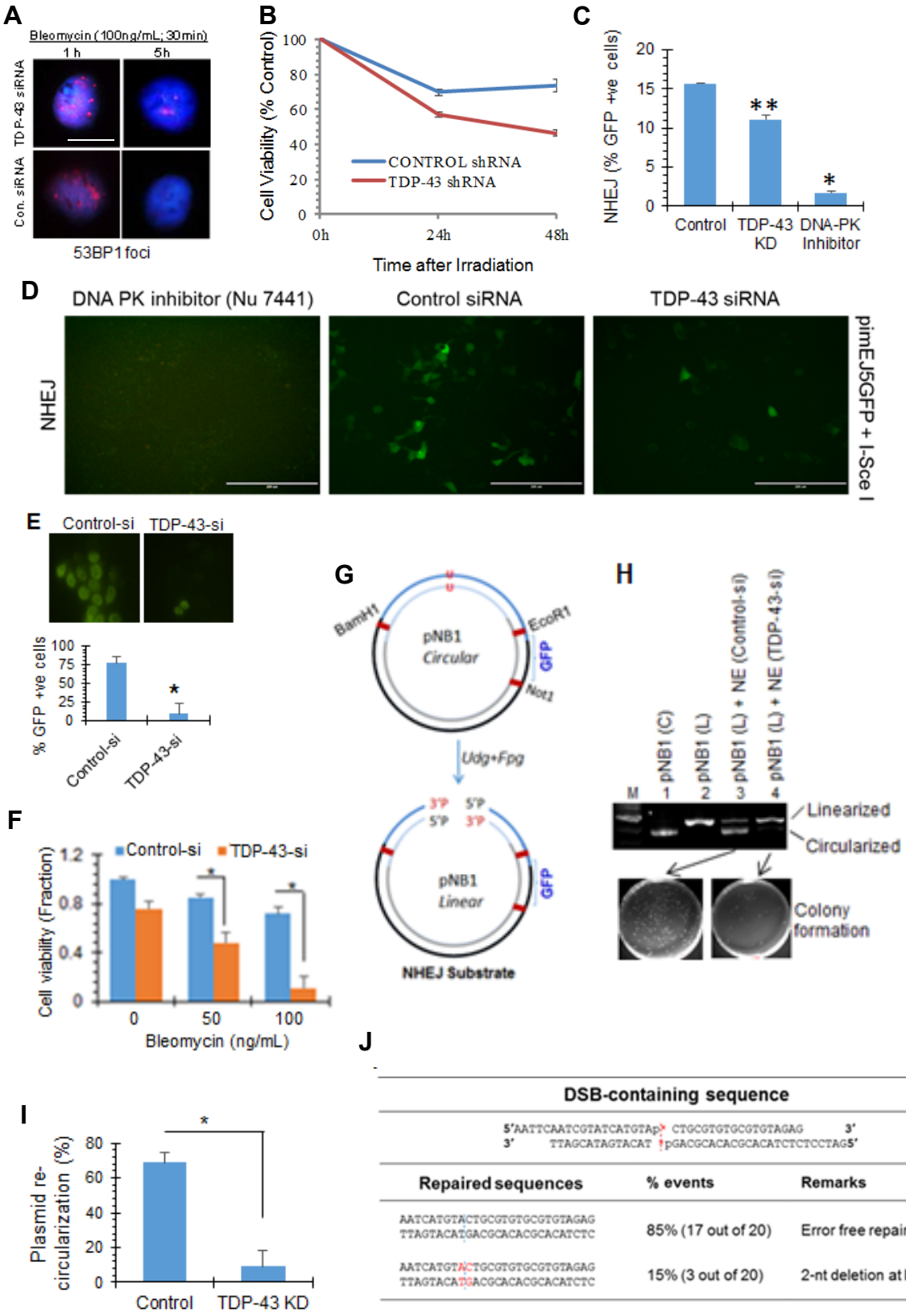
A
Bleomycin (100ng/mL; 30min)
1 h
5h
TDP-43 siRNA
Con. siRNA
53BP1 foci
B
Cell Viability (% Control)
CONTROL shRNA
TDP-43 shRNA
0h
24h
48h
Time after Irradiation
C
NHEJ (% GFP +ve cells)
Control
TDP-43 KD
DNA-PK Inhibitor
D
DNA PK inhibitor (Nu 7441)
Control siRNA
TDP-43 siRNA
NHEJ
pimEJ5GFP + I-Sce I
E
Control-si
TDP-43-si
% GFP +ve cells
F
Control-si
TDP-43-si
Cell viability (Fraction)
Bleomycin (ng/mL)
G
BamH1
EcoR1
Not1
GFP
pNB1
Circular
Udg+Fpg
pNB1
Linear
NHEJ Substrate
H
M
pNB1 (C)
pNB1 (L)
pNB1 (L) + NE (Control-si)
pNB1 (L) + NE (TDP-43-si)
Linearized
Circularized
Colony formation
I
Plasmid re-circularization (%)
Control
TDP-43 KD
J
DSB-containing sequence
5'AATTCAATCGTATCATGTAp CTGCGTGTGCGTGTAGAG 3'
3' TTAGCATAGTACAT pGACGCACACGCACATCTCTCCTAG5'
Repaired sequences
% events
Remarks
AATCATGTACTGCGTGTGCGTGTAGAG
TTAGTACATGACGCACACGCACATCTC
85% (17 out of 20)
Error free repair
AATCATGTACTGCGTGTGCGTGTAGAG
TTAGTACATGACGCACACGCACATCTC
15% (3 out of 20)
2-nt deletion at break site

Fig. S8. TDP-43 is required for DSB repair via NHEJ in neuronal genomes. (Related to Fig. 4.). (*A*) IF of 53BP1 foci in control or TDP-43 siRNA treated SH-SY5Y cells at 1h (left) and 5h (right) after bleomycin treatment. (Scale bars: 10μm.). (*B*) Neural stem cells were transduced with control or TDP-43 shRNA producing lentiviral vector, then cell viability was measured following IR treatment at the indicated time-points. (*C* and *D*) I-SceI-based NHEJ assay in HEK293 cells. Percentage of GFP+ve cells indicating NHEJ repair events measured by flow cytometry in control and TDP-43 siRNA KD cells using DNA-PKcs inhibitor (NU7441) for positive control (*C*). (*D*) IF for GFP+ve cells for indicated treatments. (Scale bars: 200μm.). (*E*) TDP-43 KD affects *in cell* DSB repair. The DSB containing plasmid substrate pNB-1 was transfected in SH-SY5Y cells 48 h after TDP-43 KD by siRNA. The GFP expression was examined 6h after pNB-1 transfection. Histogram (*Bottom*) shows quantitation of GFP positive cells. (Scale bars: 100μm.). (*F*) Viability analysis of TDP-43 siRNA-transfected NPCs at indicated doses of bleomycin. (*G-I*) *In vitro* plasmid re-circularization assay with or without TDP-43 using a non-ligatable termini containing plasmid. (*G*) Schematic of a DSB repair assay using a pNB1 plasmid with blocked (3'P) termini. (*H*) Linearized pNB1 plasmid was incubated with nuclear extracts from control or TDP-43 siRNA transfected cells for 15min at 25°C, then resolved in 1% agarose gel (*Top*), and transformed in *E.coli* for bacterial colony formation assay (*Bottom*). (*I*) Quantitation of plasmid re-circularization efficiency by colony formation assay. *, $p<0.01$. Data are presented as mean ± s.d. P values are based on two-way ANOVA. (*J*) The re-circularized plasmids were then isolated as Hirt supernatant, transformed in *E. coli*. Individual colonies were sequenced, which showed ~85% error-free repair and ~15% re-circularized sequences with one base deletion. Data are presented as means ± s.d. P values are based on two-way ANOVA: *, $p<0.01$.; **, $p<0.05$.

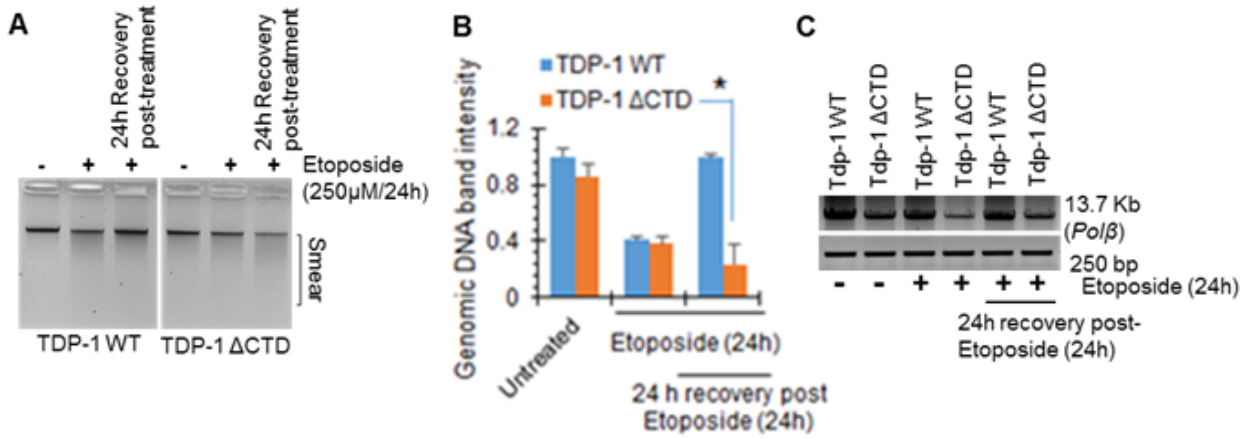

Fig. S9. Functional mutation of endogenous TDP-1 induces genomic instability in *C. elegans*. (Related to Fig. 5.). (*A* and *B*) Genomic DNA isolated from WT and mutant worms with or without Etoposide (250μM/24h) treatment analyzed by 1% agarose gel electrophoresis. The worms were treated with etoposide for 24h and recovery was measured at 48h (*A*). Quantitation of intact genomic DNA band intensity (*B*). (*C*) 13.7Kb region of *polβ* gene was amplified for DNA integrity measurement by LA-PCR analysis of the indicated genomic DNA samples, resolved in 1% agarose gel related to Fig. 5*D*.

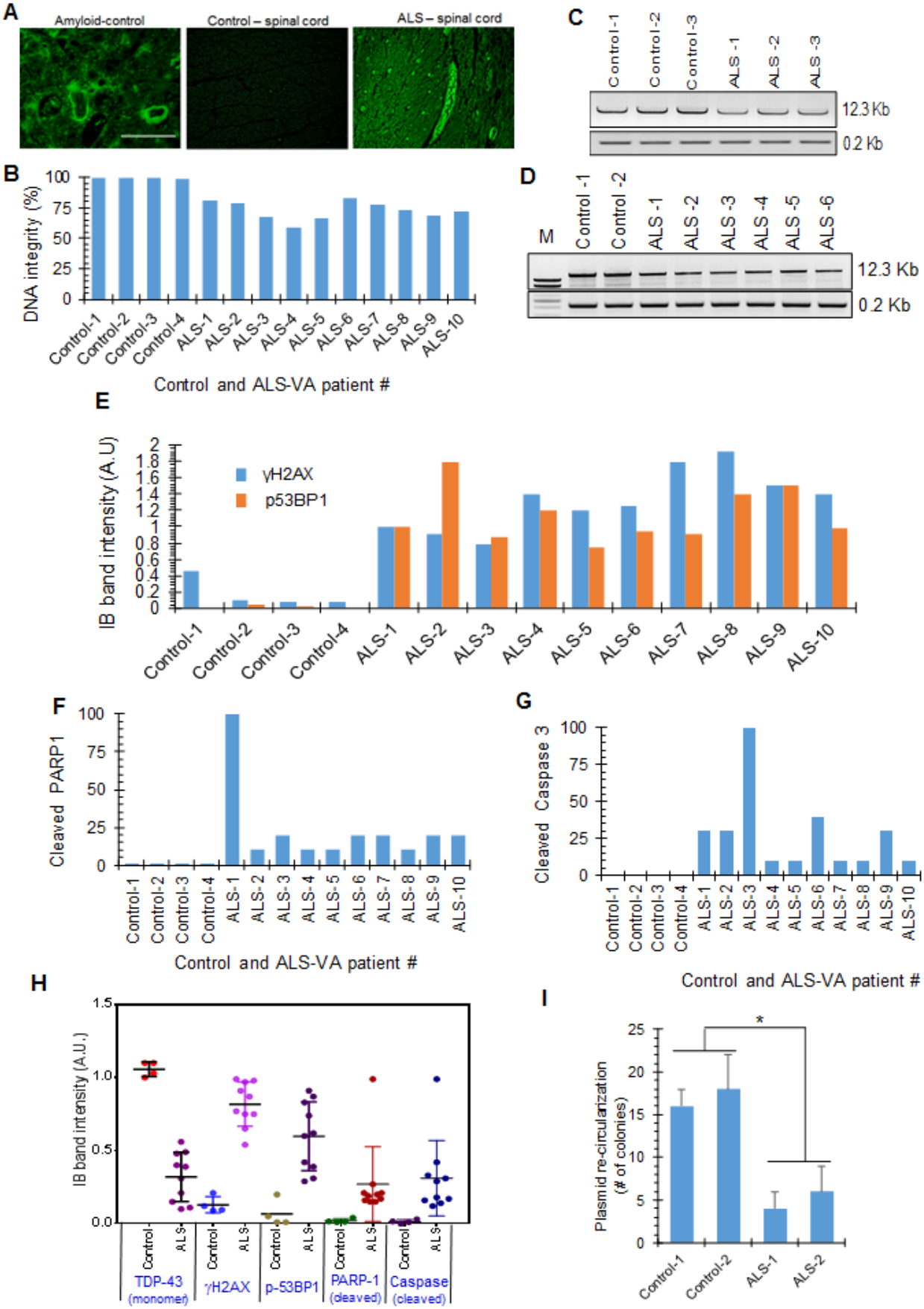
A
Amyloid-control
Control – spinal cord
ALS – spinal cord
B
DNA integrity (%)
Control-1
Control-2
Control-3
Control-4
ALS-1
ALS-2
ALS-3
ALS-4
ALS-5
ALS-6
ALS-7
ALS-8
ALS-9
ALS-10
Control and ALS-VA patient #
C
Control-1
Control-2
Control-3
ALS -1
ALS -2
ALS -3
12.3 Kb
0.2 Kb
D
M
Control -1
Control -2
ALS -1
ALS -2
ALS -3
ALS -4
ALS -5
ALS -6
12.3 Kb
0.2 Kb
E
IB band intensity (A.U)
γH2AX
p53BP1
F
Cleaved PARP1
Control and ALS-VA patient #
G
Cleaved Caspase 3
Control and ALS-VA patient #
H
IB band intensity (A.U.)
Control
ALS
TDP-43 (monomer)
γH2AX
p-53BP1
PARP-1 (cleaved)
Caspase (cleaved)
I
Plasmid re-circularization (# of colonies)
*
Control-1
Control-2
ALS-1
ALS-2

Fig. S10. DNA damage analyses in sporadic ALS spinal cord tissues. (Related to Fig. 6.). (*A*) Representative images showing Thioflavin-S staining of human brain Amyloid aggregates (reference control, *Left*), age-matched control (*Middle*) and ALS-affected spinal cord tissue (*Right*). (Scale bars: 200µm.). (*B-D*) LA-PCR analysis of 12.3Kb genomic DNA region of *polβ* gene amplified from genomic DNA of individual control and sporadic ALS spinal cord tissues. Representative image of 0.8% agarose gel separation of LA-PCR product for Guam (C) and sporadic ALS spinal cord from VABB (*B* and *D*) specimens. (*E*) Relative band intensity quantitation of p-53BP1 and γH2AX for IB with indicated antibody. Relative band intensity quantitation of cleaved-PARP1 (*F*) or cleaved Caspase-3 (*G*) for immunoblotting with indicated antibody. (*H*) Scatterplot representation for quantitation of IB band intensity for all the sporadic ALS samples (VABB) related to Fig. 6*D*. (*I*) Plasmid re-circularization analysis in control and VABB-sporadic ALS spinal cord tissue extracts (assayed in two groups; details in Methods & Results section) shows reduced DSB ligation activity in ALS spinal cord. *, $p<0.01$.

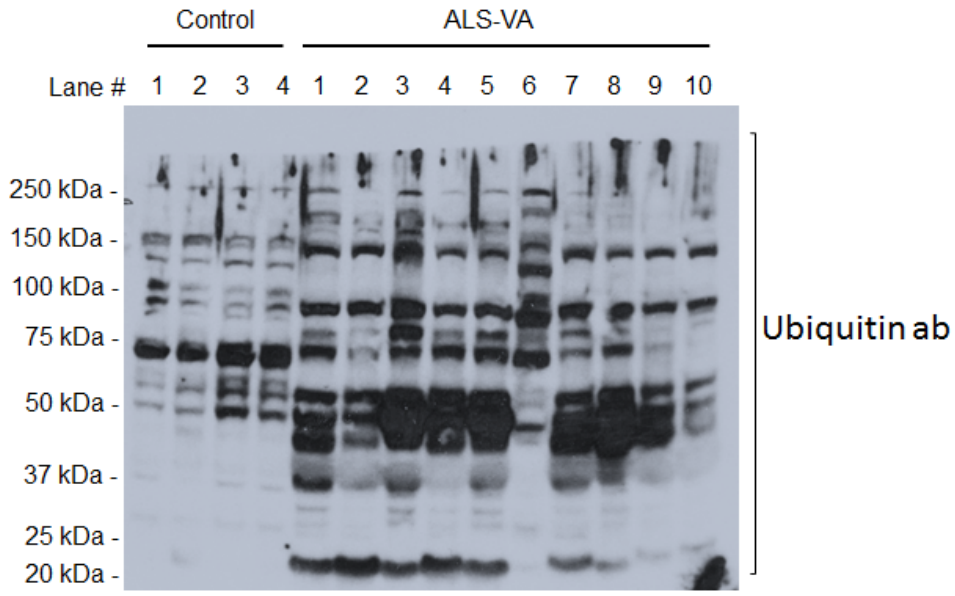

Fig. S11. Ubiquitination levels in TDP-43 proteinopathy-associated ALS spinal cord tissue. (Related to Fig. 6.). Representative IB image probed with anti-Ubiquitin antibody against the spinal cord tissue extracts from control (1-4) and ALS patients (1-10), indicating stronger ubiquitination in ALS patients.

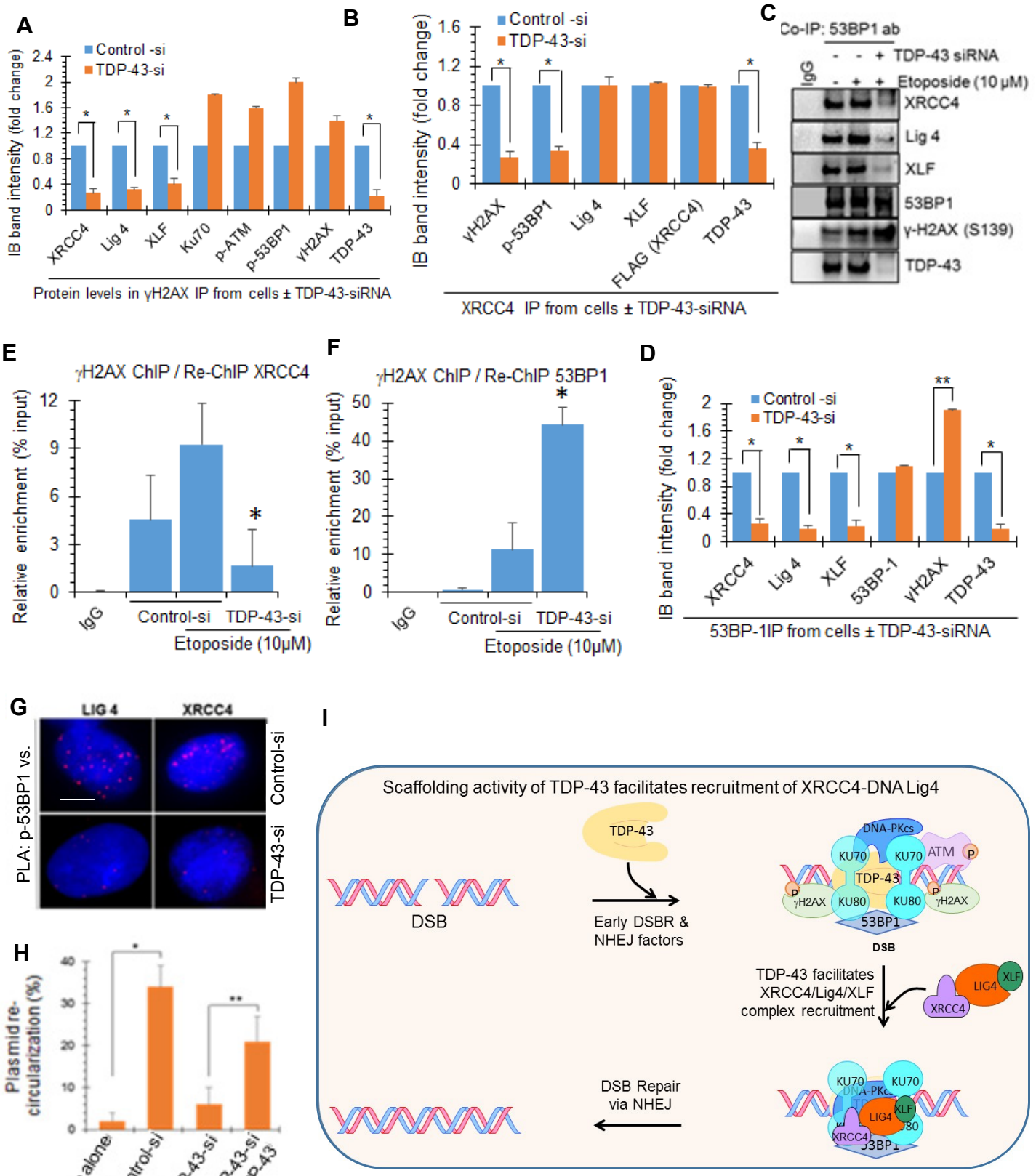
A
Control -si
TDP-43-si
IB band intensity (fold change)
XRCC4
Lig 4
XLF
Ku70
p-ATM
p-53BP1
γH2AX
TDP-43
Protein levels in γH2AX IP from cells ± TDP-43-siRNA
B
Control -si
TDP-43-si
IB band intensity (fold change)
γH2AX
p-53BP1
Lig 4
XLF
FLAG (XRCC4)
TDP-43
XRCC4 IP from cells ± TDP-43-siRNA
C
Co-IP: 53BP1 ab
TDP-43 siRNA
Etoposide (10 μM)
IgG
XRCC4
Lig 4
XLF
53BP1
γ-H2AX (S139)
TDP-43
E
γH2AX ChIP / Re-ChIP XRCC4
Relative enrichment (% input)
IgG
Control-si
TDP-43-si
Etoposide (10μM)
F
γH2AX ChIP / Re-ChIP 53BP1
Relative enrichment (% input)
IgG
Control-si
TDP-43-si
Etoposide (10μM)
D
Control -si
TDP-43-si
IB band intensity (fold change)
XRCC4
Lig 4
XLF
53BP-1
γH2AX
TDP-43
53BP-1IP from cells ± TDP-43-siRNA
G
LIG 4
XRCC4
PLA: p-53BP1 vs.
Control-si
TDP-43-si
H
Plasmid re-circularization (%)
Substrate alone
XRCC4 IP + Control-si
XRCC4 IP + TDP-43-si
XRCC4 IP + TDP-43-si + rec. TDP-43
I
Scaffolding activity of TDP-43 facilitates recruitment of XRCC4-DNA Lig4
DSB
TDP-43
Early DSBR & NHEJ factors
DNA-PKcs
KU70
KU70
ATM
P
TDP-43
γH2AX
KU80
KU80
γH2AX
53BP1
DSB
TDP-43 facilitates XRCC4/Lig4/XLF complex recruitment
LIG4
XLF
XRCC4
DSB Repair via NHEJ
KU70
KU70
LIG4
XLF
XRCC4
53BP1

Fig. S12. TDP-43 facilitates recruitment and activity of NHEJ ligation complex (XLF/XRCC4/Lig4) at DSB sites. Related to Fig. 7. (*A*) γH2AX co-IP from TDP-43 KD NPC cells (Fig. 7A) and quantitation of IB band intensity from three independent experiments. (*B*) FLAG-XRCC4 co-IP from TDP-43 KD NPC cells (Fig. 7B) and quantitation of IB band intensity from three independent experiments. (*C* and *D*) Nuclear lysates from TDP-43-siRNA-transfected NPC cells were subjected to IP with control IgG or anti-53BP1 antibody, and co-IP elutes were probed with indicated antibodies. Quantitation of IB band intensity from three independent experiments (*D*). *, p<0.01. (*E* and *F*) ChIP analysis with anti-γH2AX and re-ChIP with anti-XRCC4 antibody shows reduced fold enrichment of XRCC4 in TDP-43 KD cells (*E*). Re-ChIP with anti-53BP1 antibody showed increased fold enrichment of 53BP1 indicating enhanced DSB accumulation (*F*). *, p<0.01. (*G*) PLA of XRCC4 or Lig4 versus p-53BP1 in NPCs show reduced association after TDP-43 KD by siRNA. Representative images shown. Quantitation in Fig. 7*C*. (*H*) NHEJ ligation activity measured by plasmid re-circularization using XRCC4 co-IP elutes with or without recombinant TDP-43. *,p<0.01; **, p<0.05. Data are presented as means ± s.d. P values are based on two-way ANOVA. (*I*) Schematic model showing how TDP-43 facilitates recruitment and activity of XLF/XRCC4/Lig4 complex for NHEJ repair in neurons.

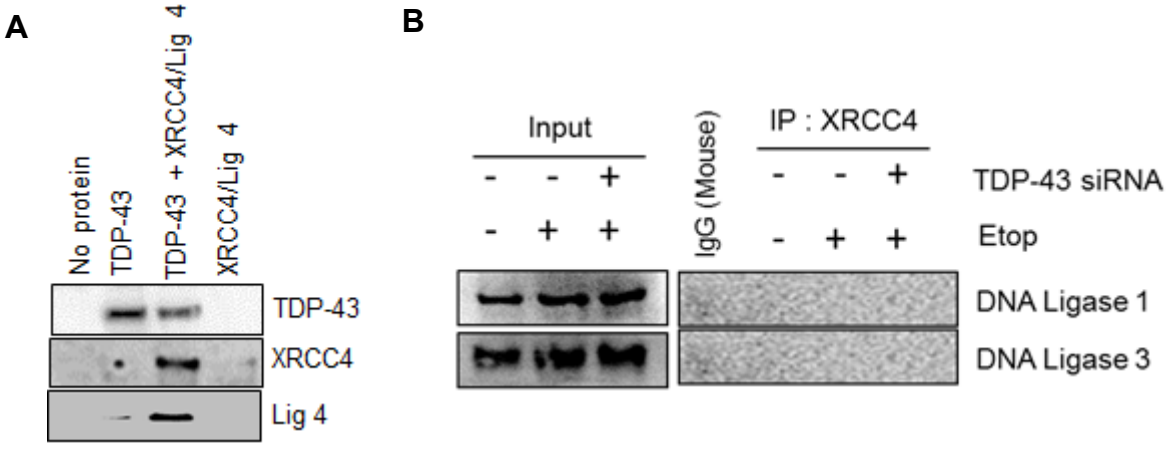

Fig. S13. Specific interaction of NHEJ factors. (Related to Fig. 7). (*A*) *In vitro* binding of recombinant TDP-43 with XRCC4/Lig4 complex, tested by His-affinity co-elution assay, then immunoblotted with anti-TDP-43, anti-XRCC4 and anti-Lig4 antibody. (*B*) neuronal cells were transfected with control or TDP-43 siRNA followed by treatment with Etoposide or vehicle. Total cell lysates were subjected to IP with control IgG or anti-XRCC4 antibody, then probed for non-NHEJ ligases with anti-Ligase1 and anti-Ligase3 antibody.